

Stress Corrosion Cracking of Candidate Alloys for the Supercritical Water Reactor Concept

**Annual Report
2006**

University of Michigan

**Gary S. Was, PI
Sebastien Teysseyre
Qunjia Peng**

Summary

Twenty-one tensile samples of alloy JPCA irradiated in FFTF in a temperature range 390-520°C and over a dose range 26.9-43.9 dpa were selected for testing in supercritical water. A set of procedures was established for the transportation, receipt, handling and testing of these samples in the Irradiated Materials Testing Laboratory at the University of Michigan. Four samples irradiated at 407 or 427°C were tested in deaerated SCW at 400°C and one sample irradiated at 520°C is being tested in 500°C SCW. All samples tested in 400°C SCW exhibited intergranular stress corrosion cracking, low strain to failure and low reduction in area. From existing data on the tensile behavior of this alloy tested in room temperature air, the SCW environment appears to have resulted in significant embrittlement. A crack growth rate test on a compact tension specimen of type 316 stainless steel was conducted in pure water under both subcritical and supercritical conditions. The crack growth rate during the test was measured by the reversed direct current potential drop technique. The test results showed that shifting the water condition from subcritical to supercritical significantly decreased the stress corrosion crack growth rate. The crack growth rate was further suppressed by increasing the temperature from 400/450°C up to 500°C under supercritical conditions. In addition, the effect of dissolved oxygen was to lower the crack growth rate compared to the deaerated case.

September 2006

**University of Michigan
Ann Arbor, MI 48109-2104**

Stress Corrosion Cracking of Candidate Alloys for the Supercritical Water Reactor Concept

1. Procedure for Shipping and Testing of Neutron-Irradiated Samples

Before beginning the test program on corrosion and stress corrosion cracking of neutron irradiated materials, a set of procedures was established for the transportation and handling of neutron irradiated samples. Subsection 1.1 covers specimen selection and subsection 1.2 covers the shipment of the samples to the University of Michigan, receipt of the samples, handling of the samples and disposal of the samples after testing. Subsection 1.3 covers the procedures for testing of irradiated samples. This section describes those procedures, and is prefaced with the initial irradiated sample selection that arrived in FY2006 and which constituted the first neutron-irradiated samples tested in supercritical water.

1.1 Irradiated specimen selection

A set of 21 samples was selected from the MOTA inventory at PNNL. The Japan Prime Candidate Alloy (JPCA) samples are in solution annealed (SA) and cold worked (CW) conditions and all are of the “W” type tensile sample design. The set of samples requested from PNNL covers both conditions and a dose range from 26.9 dpa to 43.9 dpa, and an irradiation temperature range from 390 to 520°C. The samples received from PNNL are shown in Table 1.

1.2 Sample transportation, receipt, and handling

1.2.1 Sample transportation and receipt

Pacific Northwest National Laboratory (PNNL) determined the isotopic composition and exposure rate (mRem/hr) for each of the 21 Prime Candidate Alloy samples. This information was used to prepare the shipping manifest required for shipments of hazardous materials in accordance with the applicable U.S. Department of Transportation (DOT) regulations. The isotopic composition and the exposure rate measurements also allowed for the evaluation of the shipping container required by the DOT regulations, i.e., Type A. . The Type A package was certified by the University of Michigan's Phoenix Memorial Laboratory as required by 49CFR173.412, *Additional Design Requirements for Type A Packages*.¹ PNNL completed the information for the Shipper's Declaration of Dangerous Goods as required by 49CFR172.202, *Description of Hazardous Material on Shipping Papers*² and 49CFR172.203, *Additional Description Requirements*³ and what markings or stickers were required as per 49CFR178.503, *Marking of Packaging*⁴ and what labels or wording were required as per 49CFR172.400, *General Labeling Requirements*⁵ and 49CFR172.403, *Class 7 (radioactive) material* were provided.⁶ Isotopic and exposure rate information provided by PNNL permitted the University of Michigan's Radiation Safety Services (RSS) department to complete the approval for receipt required by the Byproduct Materials License issued by the U.S. Nuclear Regulatory Commission. After this review, RSS sent to PNNL a document indicating that the UM can receive the materials as required by 10 CFR 30.41(c)⁷.

Packages were sent by common carrier, e.g., FedEx, once the appropriate packaging and hazardous materials manifests were prepared and reviewed as required by DOT regulations. The package was received by Radiation Safety Services on June 13 2006 in accordance with procedures implementing 10CFR20.1906, *Procedures for Receiving and Opening Packages*.⁸ The Prime Candidate Alloy samples are held by Radiation Safety Services (RSS) until they are needed for testing.

Table 1. JPCA samples received from PNNL for the UM GenIV SCWR program

Specimen ID	Alloy Description	Temperature (°C)	Dose (dpa)	Dose rate on sample vials @~1"/@ 1 foot
K K0	SA	390	26.9	200/13
K K1	SA	390	26.9	
K K2	SA	390	26.9	
K K4	SA	520	33.2	120/8
K K5	SA	520	33.2	
K K6	SA	520	33.2	
K K8	SA	407	41.1	150/10
K K9	SA	407	41.1	
K L0	SA	407	41.1	
K L1	SA	427	43.9	150/10
K L2	SA	427	43.9	
K L3	SA	427	43.9	
K K0	CW	390	26.9	200/13
K K2	CW	390	26.9	
K K3	CW	390	26.9	
K K8	CW	407	41.1	160/10
K K9	CW	407	41.1	
K L0	CW	407	41.1	
K L2	CW	427	43.9	150/10
K L3	CW	427	43.9	
K L4	CW	427	43.9	

1.2.2 *Sample handling*

All handling of the samples was conducted according to the guidelines set by Radiation Safety Services at the University of Michigan. As the contact exposure rate of an individual sample was less than approximately 500 mRem/hr, samples were manually loaded into the autoclave or SEM. The personnel protection equipment for manual handling of the samples consisted of a remote tong and tweezers where possible, vinyl gloves and lab coats for contamination control, and whole body and extremity (fingers) dosimetry. All manual handling of samples was overseen by Radiation Safety Services or the staff of the Phoenix Memorial Laboratory.

If the contact exposure rate on an individual sample had been greater than approximately 500 mRem/hr, then the samples would have been transferred to the hot cell by Radiation Safety Services or the staff of the Phoenix Memorial Laboratory, where they would have been remotely loaded into the autoclave using the manipulators, and following the procedure developed in FY2005 and described later in this report. The hot cells would also have been used to handle the samples for imaging in the SEM. The staff of the Phoenix Memorial Laboratory, with 20 plus years of hot cell experience, would have performed all hot cell operations.

1.2.3 Sample disposal

Waste disposal will require further evaluation of the isotopic composition, as more detail is required than for shipping. The refinement of the isotopic composition will be done by the staff of the Phoenix Memorial Laboratory considering the constituent elements of the material in question and calculating the duration of exposure to the neutron flux and energies of the incident neutrons, Erdman⁹. The exposure to the neutron flux and the energies of the incident neutrons is estimated based upon the irradiation exposure (dpa) and the irradiation conditions at the Fast Flux Test Facility where the Prime Candidate Alloy samples were irradiated. These calculations provide a first order estimate of the isotopic composition and are refined from direct measurements which include; direct analysis using high purity germanium or other detectors to analyze the gamma spectrum being emitted to identify specific isotopes, establish ratios of isotopes, or to fully quantify isotopes, and direct measurement of exposure rates to support computational methodologies for the determination of radionuclides (e.g. MicroShield¹⁰ or hand calculations). After testing and examination of the samples post failure, the samples will be given to Radiation Safety Services for disposal by the University's Radioactive Waste Broker, currently Duratek, Inc.

1.3 Procedures for testing neutron irradiated specimens

Any evaluation of the SCC behavior of irradiated specimens will be performed according to the procedure developed for this program in FY2005 if the contact exposure rate exceed 500 mRem/hr. The complete testing procedure can be described in four steps that are overseen by a representative of Radiation Safety Services or the Phoenix Memorial Laboratory. The first step consists of loading the irradiated specimens in the autoclave in the hotcell. This loading step includes sealing the vessel, installing the heater bands and the insulation. If RSS determined that additional shielding is required, concentric shields are also be installed over the autoclave in the hotcell. Once RSS confirms that the assembly can be safely removed from the hotcell, it is rolled into the Irradiated Material Testing Laboratory (IMTL) to conduct the experiment, step 2. After test completion, the testing assembly is rolled back in the hotcell where the samples are unloaded and stored in a lead pig, step 3. The last step consists in rolling the SEM chamber in the hotcell to perform the sample analysis. The four steps are detailed below.

1.3.1 Step 1: Procedure for sample loading

1. Installation of the load frame - autoclave assembly in the hot cell and cell closure.

2. Installation of the guide board (that assists with sample assembly) on the load frame-autoclave assembly.
3. Opening of the lead pig and removal of samples.
4. Mounting samples into the clevises in a loading jig and mounting of the sample-clevis assembly into the autoclave.
5. Closure of the vessel.
6. Sealing of the vessel with the bolt tensioning system.
7. Pressurization test in the hot cell to ensure that it is free of leaks.
8. Removal of the bolt tensioning system.
9. Removal of the guide board.
10. Installation of heaters and insulation.
11. Installation of additional shielding, if necessary.
12. Control of the load frame - autoclave assembly by a representative of Radiation Safety Services or Phoenix Memorial Laboratory with authorization to remove the assembly from the hotcell.

1.3.2 Step 2: Procedure for installation of the load frame-autoclave assembly in IMTL

1. Transport of the load frame – autoclave assembly to IMTL.
2. Connection of the autoclave to the water supply, heating and pressurization system in IMTL.
3. Restriction of the area surrounding the assembly and notification of the area as containing radioactive specimen.
4. Heat up and circulation of SCW for a CERT experiment.

1.3.3 Step 3: Procedure for sample unloading after completion of the experiment

1. Placement of the load frame - autoclave assembly in the hot cell and cell closure.
2. Shield removal.
3. Removal of the insulation and heater bands.
4. Installation of the guide board
5. Installation of the bolt tensioning system and vessel opening.
6. Removal of the bolt tensioning system.
7. Removal of the vessel body.
8. Unloading the samples from the clevises and storage in individual containers
9. Loading of the containers in the lead pig
10. Hotcell opening, load frame assembly checked for contamination and removed from the hotcell.

1.3.4 Step 4: Sample observation by scanning electron microscopy

1. Installation of the SEM in the hotcell and closure of the hotcell.

2. Retrieving of tested specimen from the lead pig and insertion into the microscope chamber.
3. Sample observation using the microscope controls installed outside of the hotcell.
4. Removal of specimen from the microscope chamber and storage in the lead pig.
5. Hotcell opening and removal of the SEM after checking for contamination.

For a contact exposure rate below 500mRem/hr, samples are manually loaded, following a simplified procedure detailed below.

1.3.5 Step 1: Procedure for sample loading

1. Transport of the samples in a lead pig to IMTL by a representative of Radiation Safety Services or Phoenix Memorial Laboratory.
2. Opening of the lead pig and removal of samples.
3. Mounting samples into the clevises and mounting of the sample-clevis assembly into the autoclave.
4. Closure of the vessel.
5. Sealing of the vessel with the bolt tensioning system.
6. Pressurization test in the hot cell to ensure that it is leak free.
7. Removal of the bolt tensioning system.
8. Installation of heaters and insulation.
9. Control of the load frame - autoclave assembly by a representative of Radiation Safety Services or Phoenix Memorial Laboratory to determine the appropriate posting of the area.

1.3.6 Step 2: Procedure for sample unloading and observation by scanning electron microscopy

1. Unloading the samples from the clevises and storage in individual containers.
2. Loading of the containers in the lead pig.
3. Removing individually the sample to be observed from the lead pig and installation in the microscope chamber.
4. After observation, removal of sample from the microscope chamber and storage in the lead pig.
5. SEM chamber check for contamination.

2. CERT Experiments on Neutron Irradiated JPCA Alloys

2.1 Samples selection and alloys description

Two CERT experiments on neutron irradiated samples were performed. Stress corrosion cracking susceptibility of JPCA alloy [11] in 400°C supercritical water was investigated using samples K[L0, K[L2, K]K9, K]L2, Table 1. Those samples had been irradiated slightly above 400°C (407 and 427°C), so the test temperature of 400°C assured that the irradiated microstructure was likely to be stable during the experiment. Two slightly different doses (41.1 and 43.9 dpa) and both solution-annealed (SA) and cold-worked (CW) conditions are represented. The JPCA samples were of the “W” design with a gage section width of 0.094” and a thickness of 0.02”.

Only the set of samples irradiated at 520°C to 33.2 dpa, table 1, was suitable for the investigation of the SCC susceptibility at 500°C. This test was conducted with one irradiated sample and three unirradiated samples. The unirradiated samples were solution annealed stainless steels 316L and D9 and solution annealed nickel-base alloy 690. The unirradiated samples have the same design of the JPCA samples. However, as the yield strength of the unirradiated samples is lower to that of the irradiated samples, the thickness was increased to 0.036 mm as shown in Figure 1. Unirradiated samples were made by electric discharge machining. The machined samples were mechanically polished using standard metallographic techniques and then electropolished in perchloric acid (10%) and methanol solution maintained at -50°C using 40V for 10-20 s to obtain a mirror finish.

Most of the as-received neutron-irradiated samples were covered by varying amounts of rust as shown in Figure 2. After observation of each sample, the tested samples were selected based of the limited amount, or absence, of rust and scratches observed of the gage surface. Samples tested at 400°C are presented in Figures 3 and 4.

Table 2. Alloys tested in supercritical water.

Alloys	C	Mn	Fe	S	Si	Ni	Cr	Mo	Cu	N	Co	P	other
JPCA*	.06	1.77	Bal	.005	0.5	15.6	14.2	2.3	NM	.004	NM	.027	0.24 Ti .003 B
316L	0.022	1.86	Bal	.001	0.65	10.12	16.62	2.06	0.24	0.02	0.05	0.03	-
D9	0.04	1.97	Bal	.005	0.64	15.04	14.25	2.25	.008	.005	.008	.003	0.28 Ti 10ppm B
690	0.03	0.18	10.0	.001	0.03	Bal	29.40	0.01	0.01	NM	NM	NM	0.22 Al 0.34 Ti

NM: not measured

* from ref. [11]

Chemical compositions of the alloys are given in Table 2 and the list of the tested samples and the testing conditions is summarized in Table 3.

Table 3. Samples used in supercritical water tests and testing conditions

Sample ID	Description	Irradiation	Testing condition
K L0	JPCA - SA	41.1 dpa at 407°C	400°C deaerated SCW
K L2	JPCA - SA	43.9 dpa at 427°C	400°C deaerated SCW
K K9	JPCA - CW	41.1 dpa at 407°C	400°C deaerated SCW
K L2	JPCA - CW	43.9 dpa at 427°C	400°C deaerated SCW
K K4	JPCA - SA	33.2 dpa at 520°C	500°C deaerated SCW
316L	316L - SA	Unirradiated	500°C deaerated SCW
D9	D9 - SA	Unirradiated	500°C deaerated SCW
690	Alloy 690 - SA	Unirradiated	500°C deaerated SCW

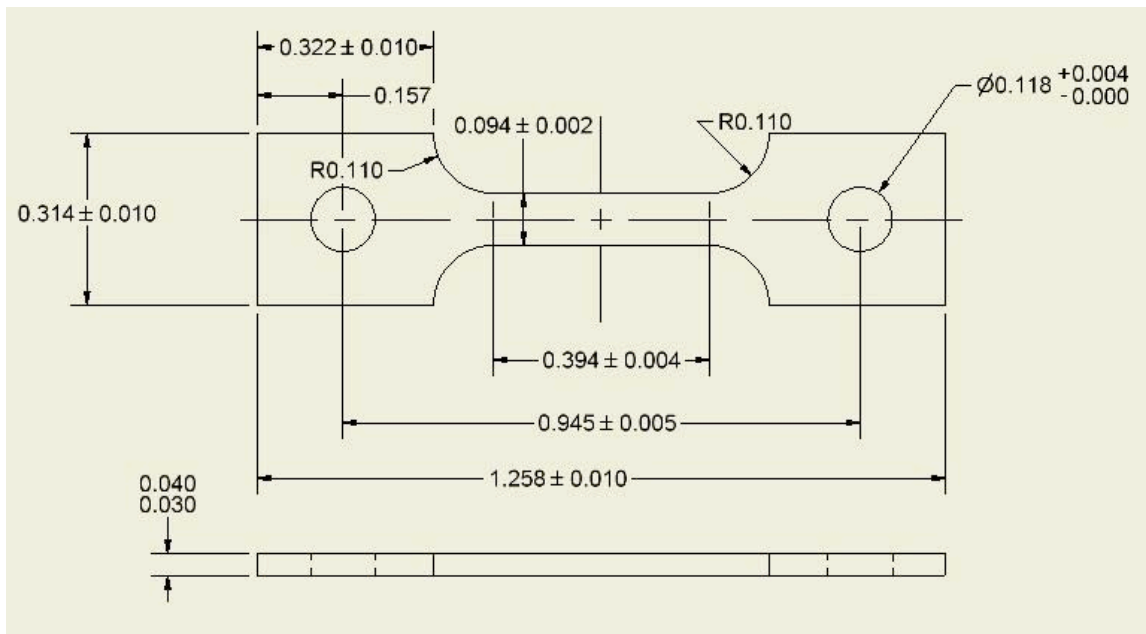


Figure 1. "W" shaped tensile sample design. Dimensions are given in inches.



Figure 2. JPCA sample K[L]0, as received from PNNL. The sample is covered with rust, from an identified source.



Figure 3. Sample K[L]0 prior to testing.

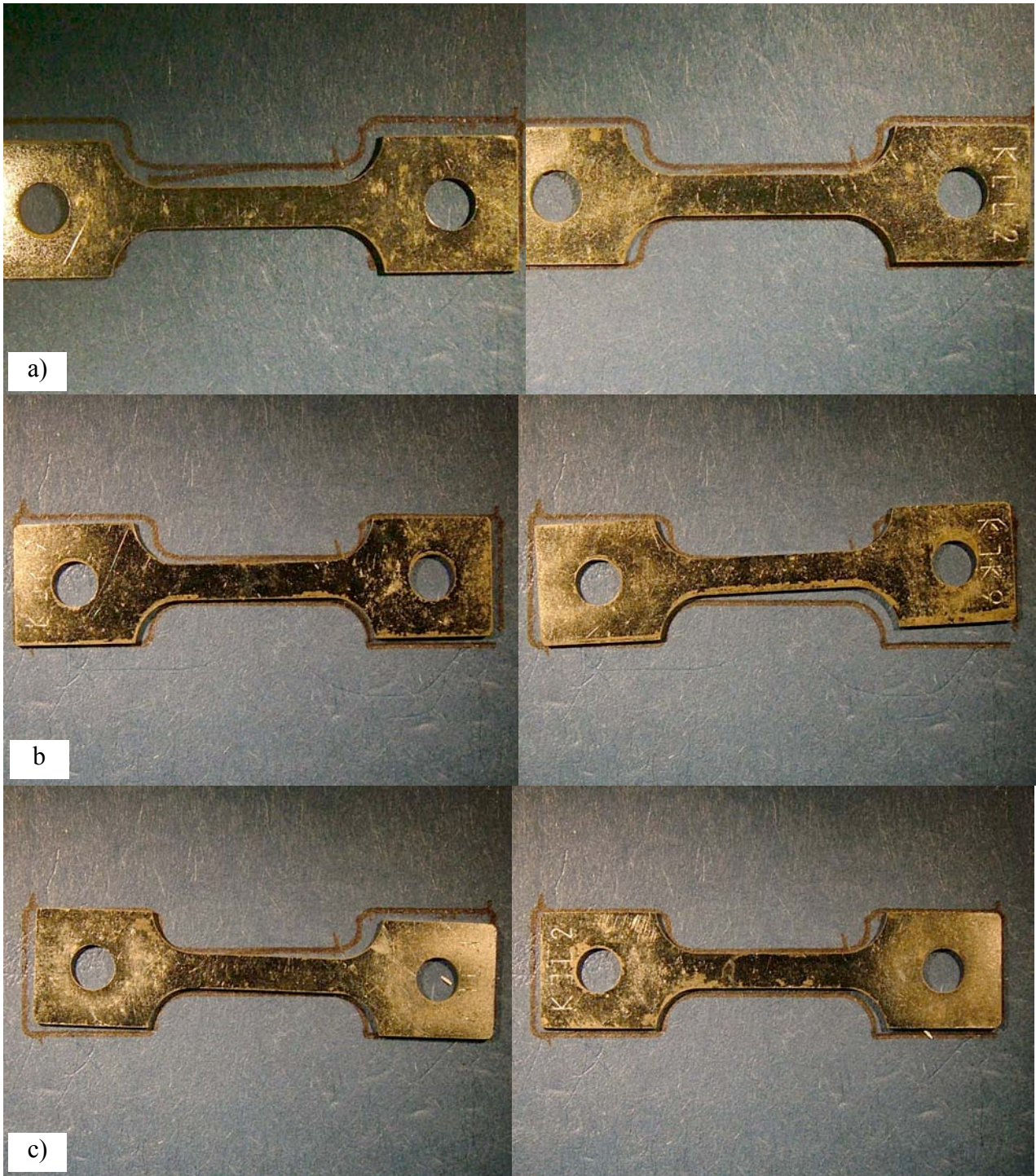


Figure 4. Samples a) K[L2, b) K]K9 and c) K]L2, prior to testing.

2.2 Samples hardness

Samples irradiated under the same condition as those to be tested in 400°C SCW were transferred to the Michigan Ion Beam Laboratory for hardness measurement. The transfer was monitored by OSEH. Hardness was evaluated by Vickers indentation with a 100g load at room temperature. Twenty indents were made at room temperature for each irradiation condition. Hardness of the alloys in different condition was measured as shown Table 4.

Table 4. Hardness measured prior to testing in SCW.

Sample ID	Description	Hardness/ standard deviation (Hv)
K K9	SA/41.1 dpa at 407°C	346.8 / 10.7
K L1	SA/43.9 dpa at 427°C	296.8 / 12.17
K L0	CW/41.1 dpa at 407°C	355.6 / 11.17
K L4	CW/43.9 dpa at 427°C	334.3 / 14.77
K K4	SA/33.2 dpa at 520°C	
316L	SA, unirradiated	150 / 5
690	SA, unirradiated	184 / 6
D9	SA, unirradiated	269 / 5

2.3 Testing condition

Constant extension rate tensile experiments were performed in the refreshed SCW system built for this project and validated in 2005 as described in the FY2005 report. [13] The experiments were conducted in the deaerated condition ($O_2 < 10$ ppb). The conductivity in the outlet water was maintained below $0.1 \mu\text{S}/\text{cm}$ for all tests. The experiments were performed at 400°C and 500°C under 3450 psi of pressure. The internal pressure applied a stress on the samples estimated to be 329 MPa or the “K” series neutron irradiated samples. Stable water chemistry was achieved in approximately 12 hours, after which the samples were strained at a nominal rate of $3 \times 10^{-7} \text{ s}^{-1}$. Nominal testing conditions are summarized in Table 5.

Table 5. Nominal SCW testing conditions

Environment	Phase	Supercritical water
	Temperature	400°C
	Pressure	3450 psi
	Conductivity	<0.1 $\mu\text{m}/\text{cm}$
	DO	< 10 ppb
Deformation	CERT at $3 \times 10^{-7} \text{ s}^{-1}$	

2.4 Results

2.4.1 *Specific procedures*

During the experiment, the facility was regularly surveyed for contamination of the water loop. A 500 ml water sample was drawn from the on-service water column on a weekly basis by

RSS, to be counted for radioactivity using a germanium detection system. In addition, the 2 micron and 0.5 micron filters and the ion exchanger were surveyed using a Geiger Mueller pancake probe in fast response mode with audible output in order to detect any increase in the audible count rate. During the course of the experiment, both measurements established that the water loop remained uncontaminated. After the completion of the experiment, it was found that the inside bottom of the autoclave and the clevises were slightly contaminated. The system was decontaminated and received a clean label from RSS.

After SEM observation, all areas of the chamber that were in contact with the radioactive samples were swiped with a wet cotton swab and checked for contamination. It was determined that the SEM has not been contaminated during operation.

2.4.2 400°C experiment results and discussion

Stress-strain behavior

Stress-strain curves obtained from all four samples are presented in Fig. 5. The stress applied due to the internal pressure (329 MPa) was added to the measured stress to arrive at the total stress experienced by the samples. All four samples exhibited very high yield strength and a low strain to rupture. The solution annealed samples, K[L0 (407°C/41.1 dpa) and K[L2 (427°C/43.9 dpa) exhibited a similar yield stress (760 and 762 MPa, respectively). Sample K]L2 (CW-427°C/43.9 dpa) showed a higher yield stress (800 MPa) which is similar to the maximum stress reached by sample K]K9 (CW-407°C/41.1 dpa), 850 MPa. The shape of the curve obtained with sample K]K9 made it difficult to determine if the stress decreased just after the YS was reached or if the sample started to fail before reaching the YS.

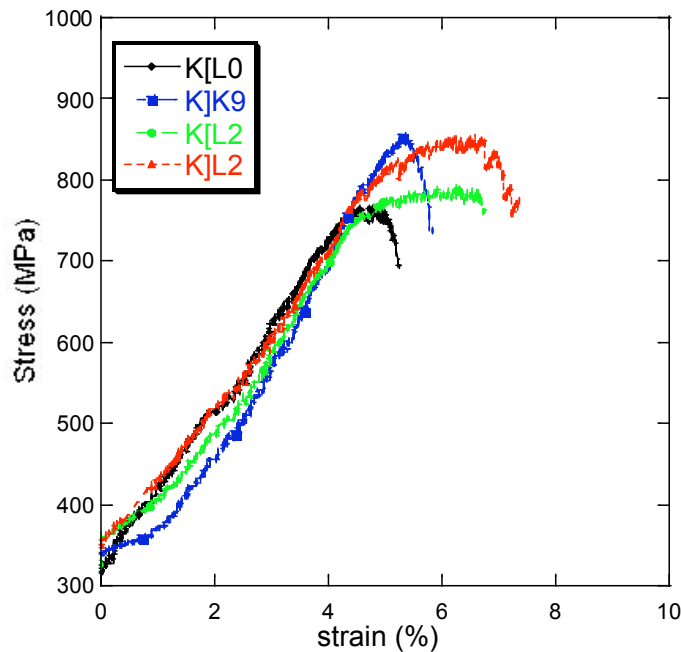


Figure 5. Stress-strain curves obtained in CERT experiment in 400°C deaerated SCW at a strain rate of $3 \times 10^{-7} \text{ s}^{-1}$.

Samples irradiated to 43.9 dpa at 427°C (sample K[L2 and K]L2) exhibited some strain hardening after yielding, whereas the samples irradiated to 41.1 dpa at 407°C, K[L0 and K]K9, exhibited a decrease of stress just after the YS was reached. Sample K]L2, irradiated to 43.9 dpa at 427°C failed after about 2.5% plastic strain (about 7% total strain) whereas sample K]K9, irradiated to 41.1 dpa at 407°C failed after about 1.5% plastic strain (about 5% total strain). Table 6 show a summary of the results of the constant extension rate experiment performed in 400°C deaerated SCW. It is important to note, however, that given the elastic modulus of 200GPa, the elastic strain is approximately 0.4%, so that much of the reported total strain is compliance of the loading system.

The results should be compared with room temperature stress-strain behavior (strain rate of $6.7 \times 10^{-7} \text{ s}^{-1}$) obtained by Kohno [12] of JPCA alloy irradiated at 427°C to 43.9 dpa. The YS was reported to be between 700 and 750 MPa, which is consistent with our results. It was also reported that the samples reached an ultimate tensile strength of 900 MPa and that they failed by 10% strain. This comparison indicates an effect of the environment on the behavior of the alloys.

Table 6. Summary of CERT experiments in deaerated SCW at 400°C.

Sample	Condition	Yield stress (MPa)	Max stress (MPa)	Strain to failure total/plastic (MPa)
K[L0	SA-407°C/41.1 dpa	760	766	5.25/1.5
K]K9	CW-407°C/41.1 dpa	850	850	5.70/1.5
K[L2	SA-427°C/43.9 dpa	762	785	6.75/2.2
K]L2	CW-427°C/43.9 dpa	800	844	7.25/3.0

2.4.3 *Post-test sample analysis*

Sample K[L0 (SA-407°C/41.1 dpa)

Necking was very minimal on this sample. No cracking was observed away from the main crack but secondary intergranular cracking was observed in the proximity of the fracture surface as shown in Fig. 6. Approximately 20% of the fracture surface was characterized by intergranular cracking, as shown in Fig. 7. The fracture behavior is summarized in Table 7.

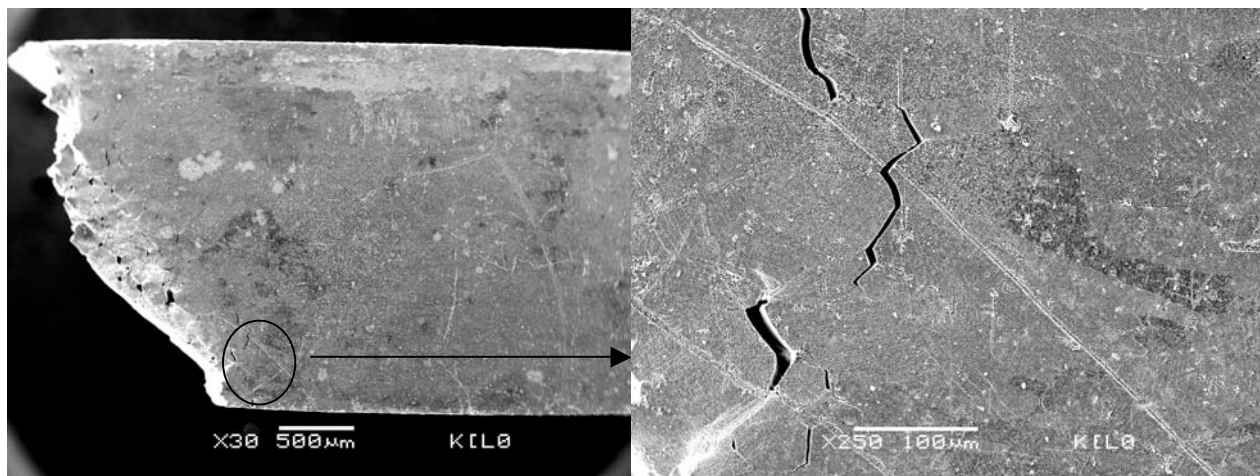


Figure 6. Gage surface of sample K[L0 (SA-407°C/41.1 dpa) after testing in 400°C deaerated SCW.

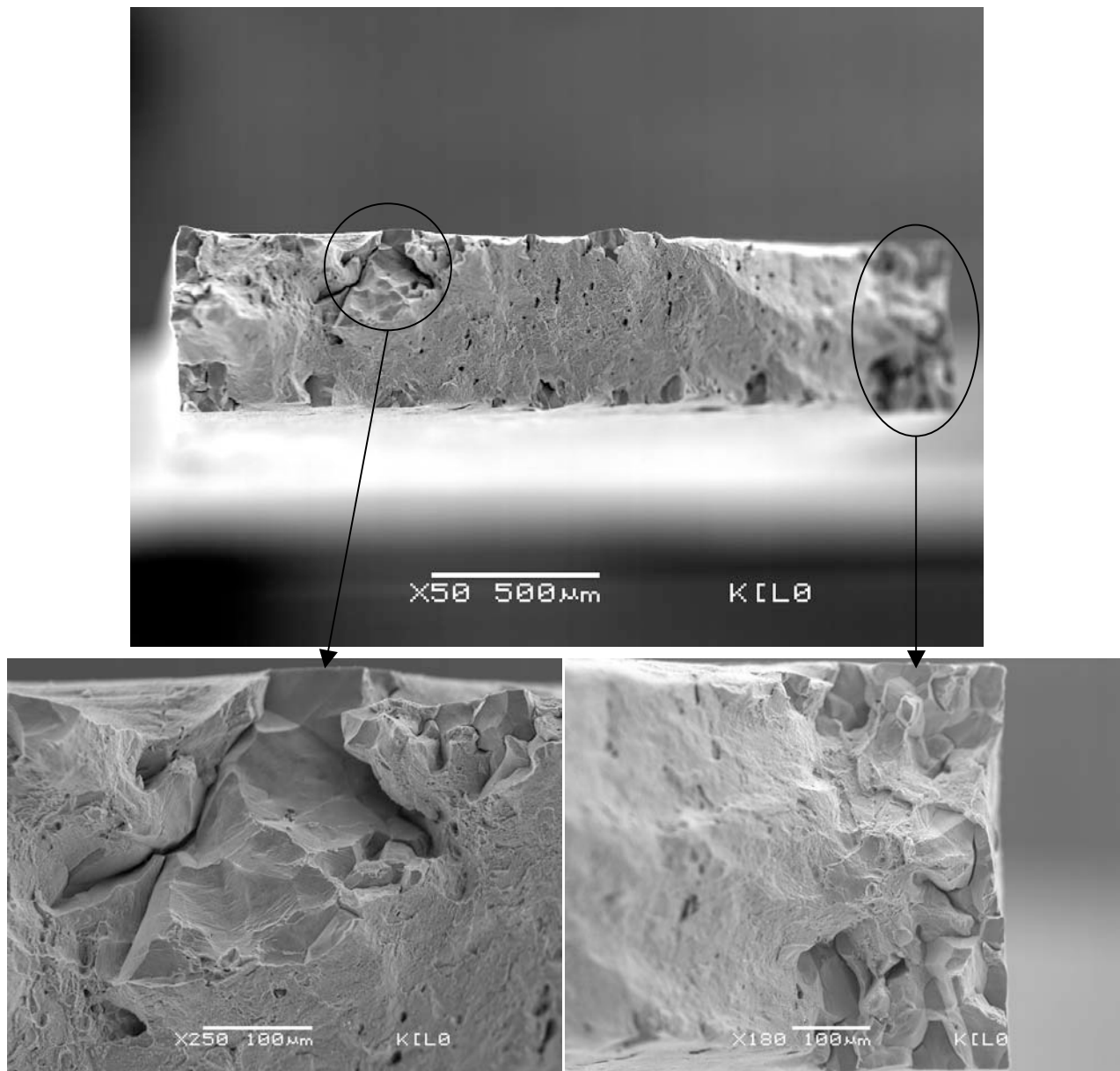


Figure 7. Fracture surface of sample K[L0 (SA-407°C/41.1 dpa) after testing in 400°C deaerated SCW.

Sample K[L2 (SA-427°C/43.9 dpa)

Necking was more prominent on this sample than on solution annealed sample K[L0. While cracking on the gage surface cracking occurred mostly near the fracture surface, a few cracks were observed away from the main crack as shown in Fig. 8. The fracture surface contained about 7.5% of intergranular cracking, Fig. 9.

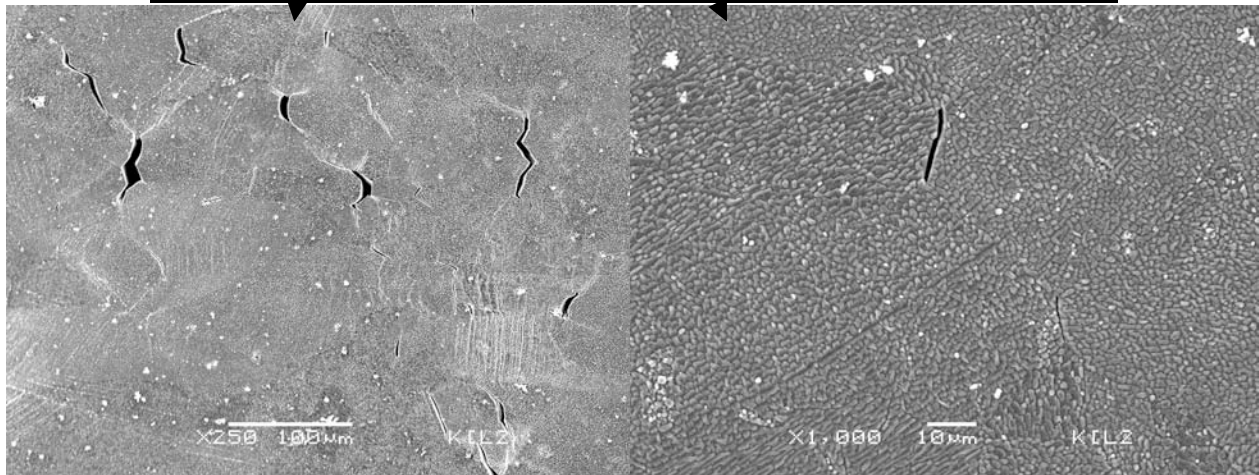
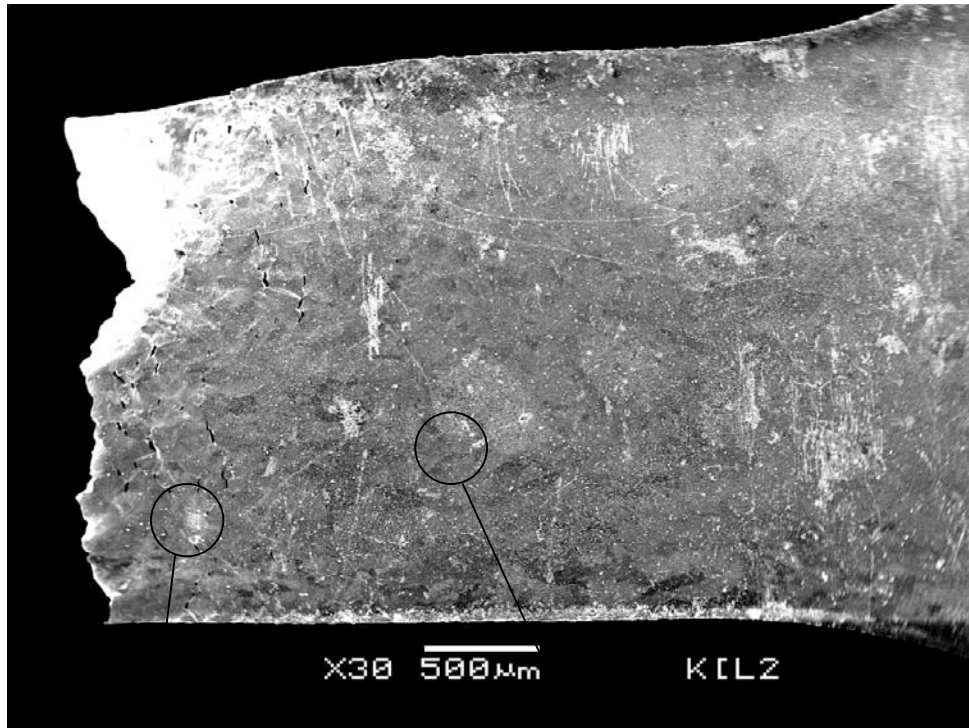


Figure 8. Gage surface of sample K[L2] (SA-427°C/43.9 dpa) after testing in 400°C deaerated SCW.

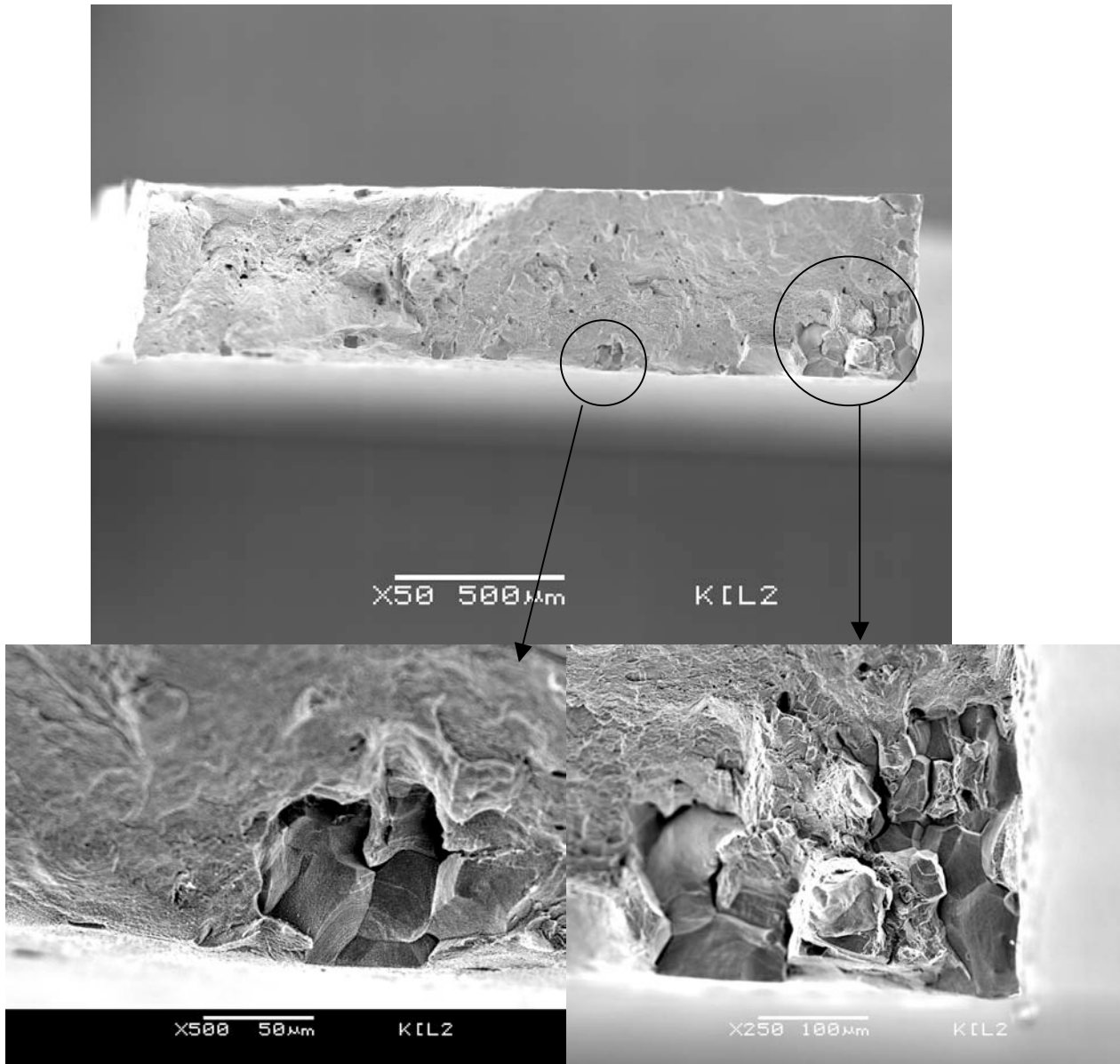


Figure 9. Fracture surface of sample K[L2 (SA-427°C/43.9 dpa) after testing in 400°C deaerated SCW.

Sample K[L2 (CW-427°C/43.9 dpa)

Minimal necking occurred on this sample. However, it appeared that the reduction of cross section was more significant on this sample than on the solution-annealed samples. Most of the secondary cracks were near the fracture surface, but some cracks were also observed further away as shown in Fig. 10. Analysis of the fracture surface revealed that intergranular cracking accounted for approximately 13.7% of the area, Fig. 11.

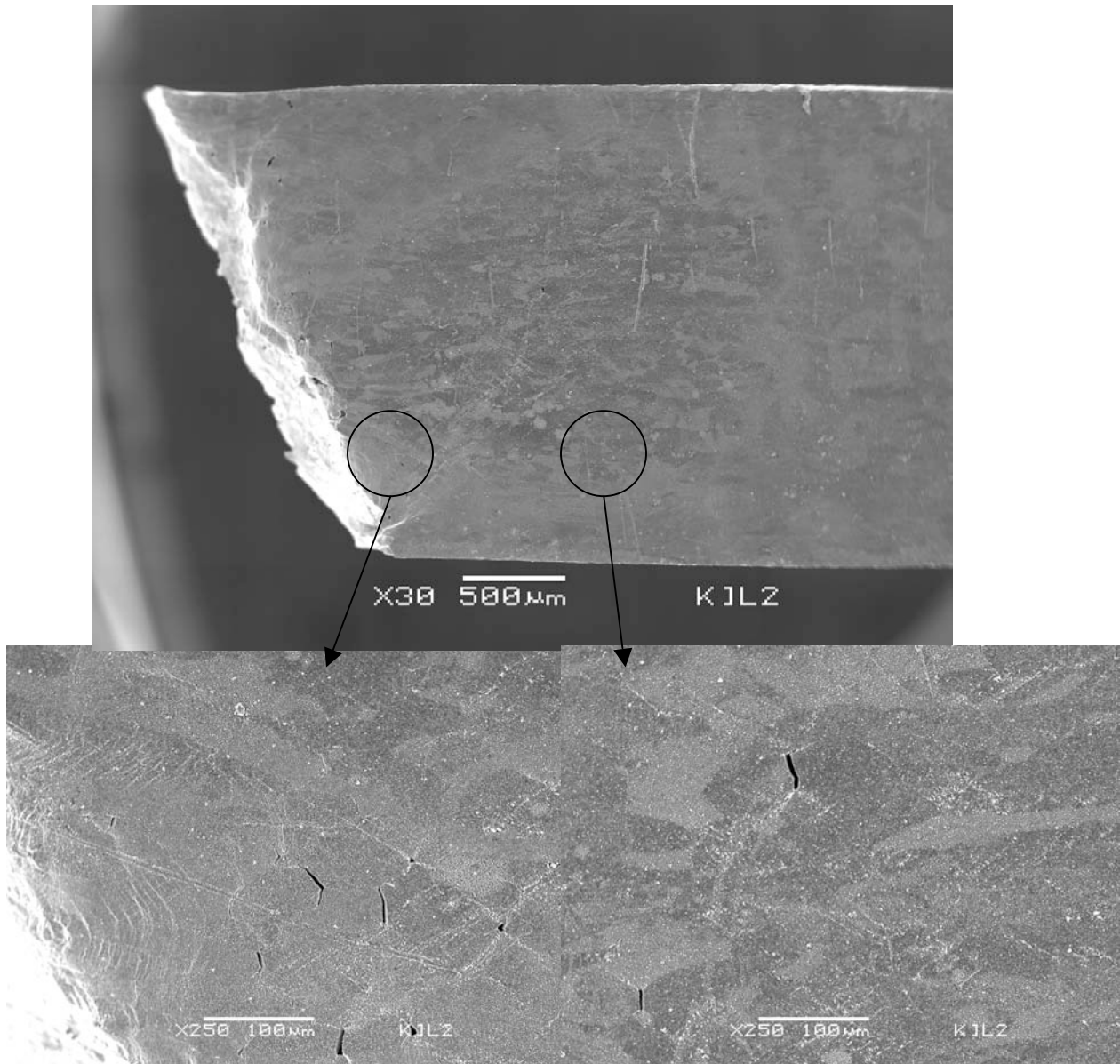


Figure 10. Gage surface of sample K]L2 (CW-427°C/43.9 dpa) after testing in 400°C deaerated SCW .

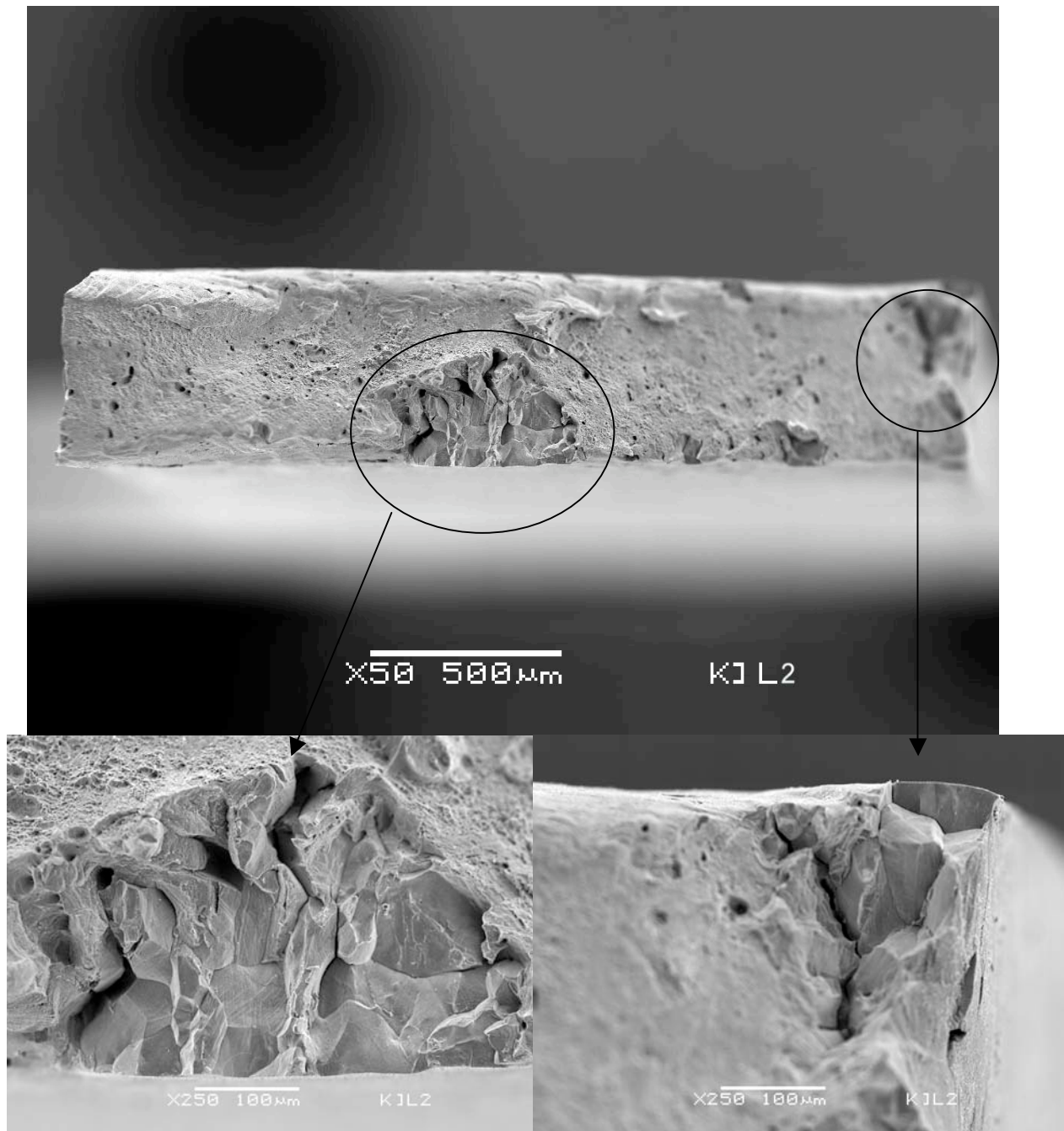


Figure 11. Fracture surface of sample KJL2 (CW-427°C/43.9 dpa) after testing in 400°C deaerated SCW.

Sample K]K9 (CW-407°C/41.1 dpa)

Observation revealed that sample K]K9 did not fail in the gage section. As shown of Fig. 12, the failure occurred at the pin-hole. There was no evidence of cracking on the gage surface. The pin-hole area that did not fail did not show any evidence of deformation or cracking. Three cracking zones were observed around the cracked pin-hole: one on each side of the hole, and one at the “bottom” on the hole (where the pin pulled through). Each zone showed evidence of intergranular cracking near the main crack as shown on Fig. 13.

The fracture surface observation showed that the cracked region located at the bottom (area 3 on Fig. 12) was 100% intergranular as shown in Fig. 14. The crack propagated in several directions, as shown on Fig. 15.

As the conditions that led to cracking were not controlled and the loading mode involved significant bending stress, it is not possible to compare the %IG obtained in this test with other experiments. However, the susceptibility to IG cracking under a multiaxial stress state is clearly evident.

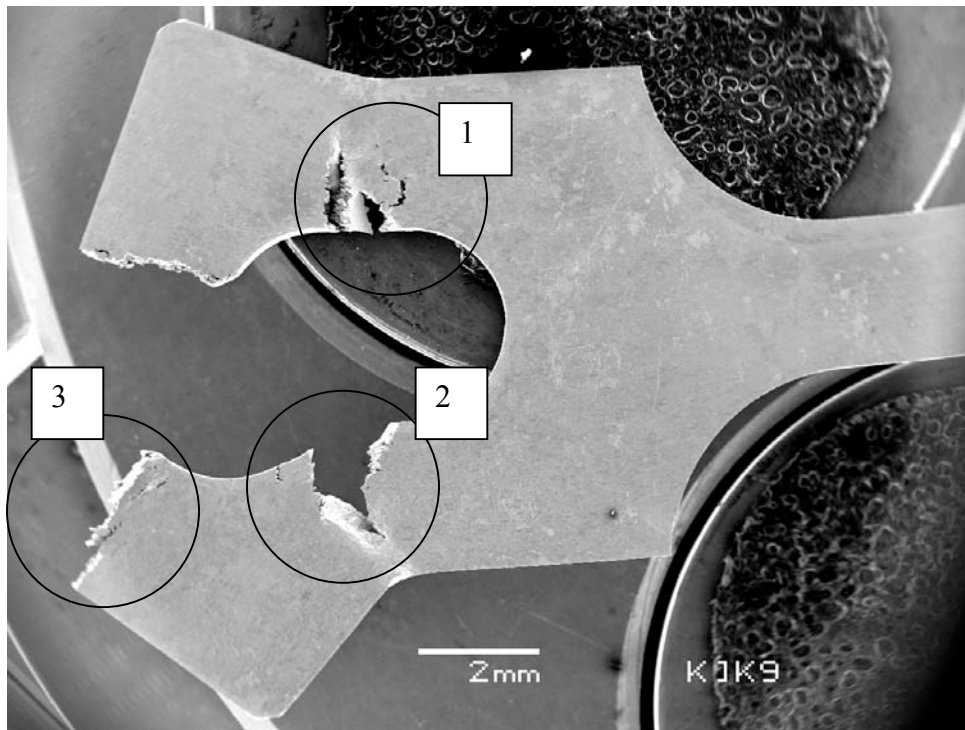


Figure 12. Sample K]K9 (CW-407°C/41.1 dpa) after completion of the test. The sample failed at the pin-hole.

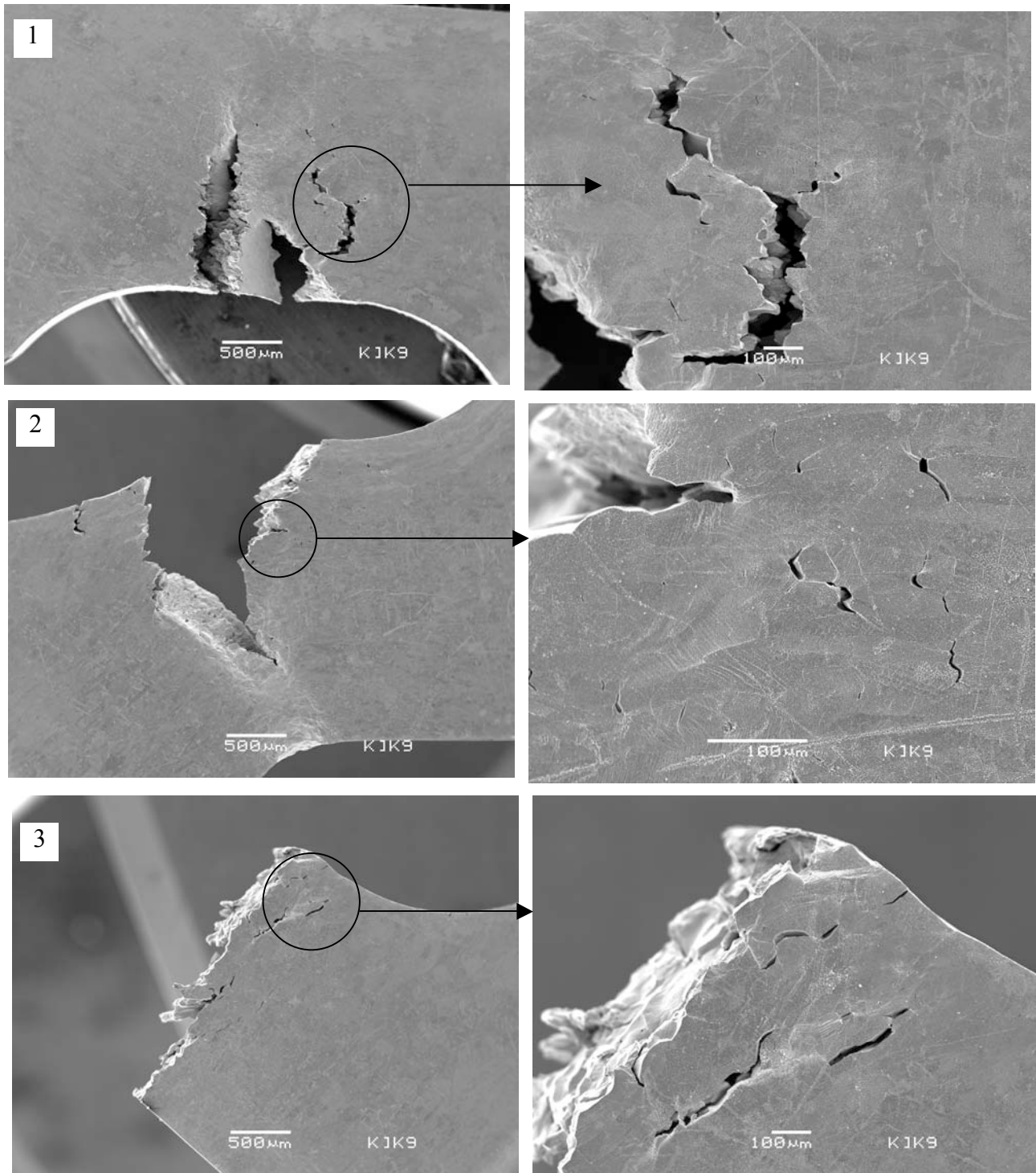


Figure 13. Details of the three main regions around the pinhole of sample KJK9 (CW-407°C/41.1 dpa) where cracking was observed.

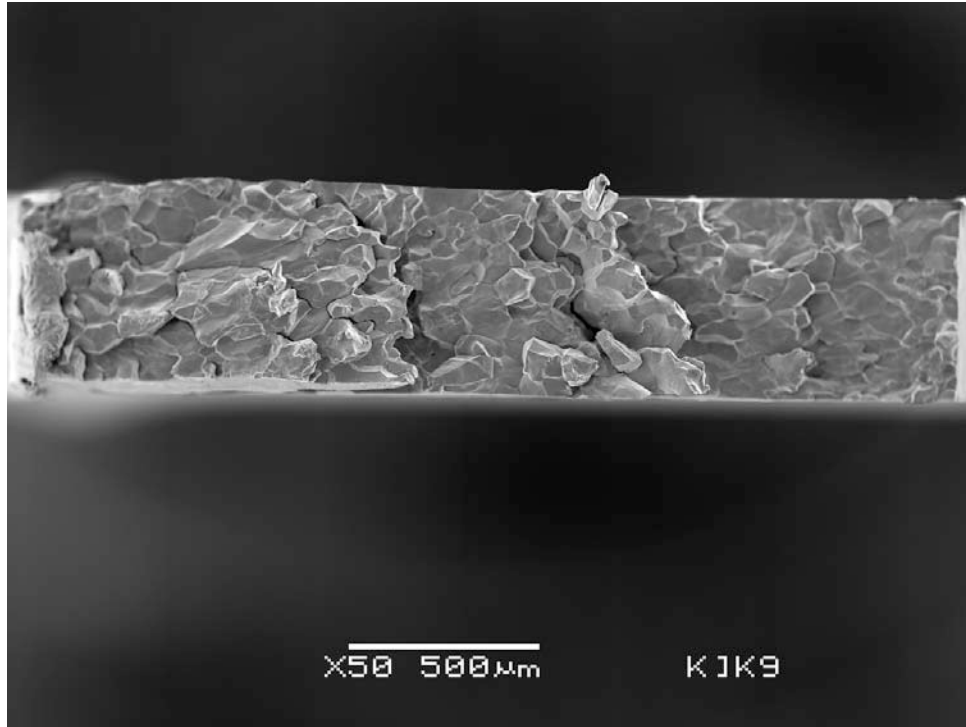


Figure 14. Fracture surface of sample KJK9 (CW-407°C/41.1 dpa) after CERT experiment in 400°C deaerated SCW, showing that the cracking is completely intergranular.

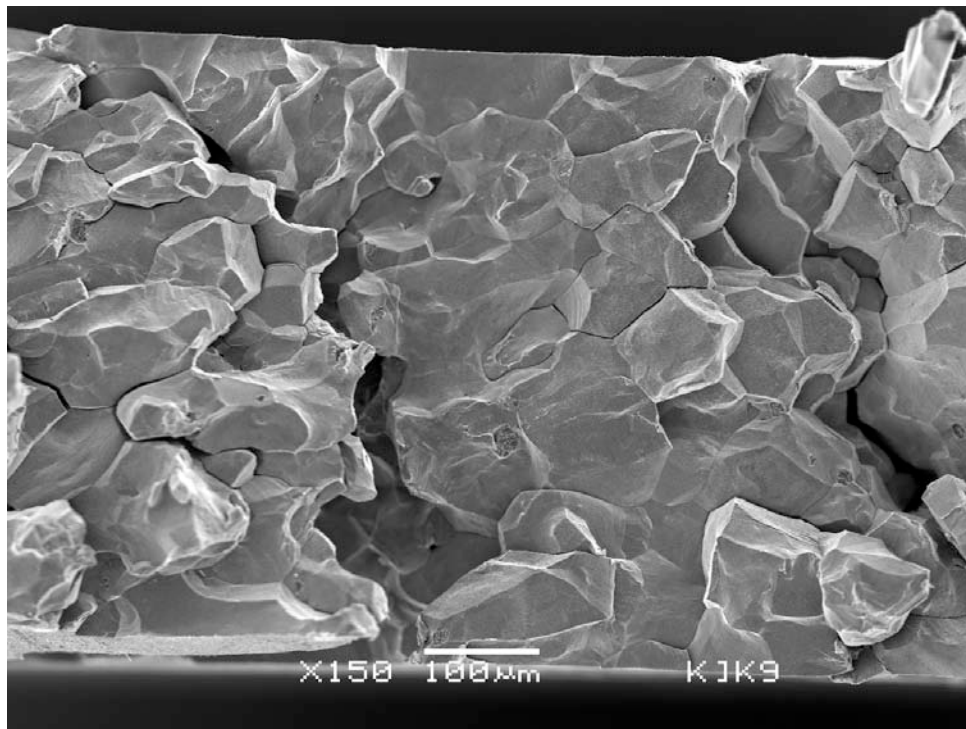


Figure 15. Detail of the fracture surface of sample KJK9 (CW-407°C/41.1 dpa) showing crack branching.

Table 7. Summary of fracture behavior of samples tested in deaerated, 400°C SCW at 400C.

Sample	Description	Reduction in area (%) [*]	%IG cracking	Remarks
K[L0	SA-407°C/41.1 dpa	6	20	No cracks far from fracture surface
K]K9	CW-407°C/41.1 dpa	NA	100	Did not fail in the gage section
K[L2	SA-427°C/43.9 dpa	7	7	Few cracks away for fracture surface
K]L2	CW-427°C/43.9 dpa	11	13.7	Some cracks away for fracture surface

2.4.4 500°C experiment

The experiment at 500°C is in progress at the time of this writing, and should be nearing completion by the end of the FY. Results on that test will be reported in the FY2007 annual report.

2.5 Summary

All specimens exhibited IG cracking. K]K9 failed at a pinhole, but no evidence of deformation or cracking in this area was observed for the other samples. It appears that samples irradiated at 407°C to 41.1 dpa exhibited less elongation to rupture, less reduction of area and more %IG cracking than their counterparts irradiated at 427°C to 43.9 dpa. Cold work had a negative effect on IASCC as cold worked samples exhibited more intergranular cracking than their solution-annealed counterparts.

3. Benchmark Crack Growth Rate Test

The objective of this test is to determine the stress corrosion crack growth rate of austenitic alloys in supercritical water. The focus of the immediate study is the temperature dependence of crack growth rate across the subcritical-supercritical transition and the effect of dissolved oxygen in supercritical water. A constant stress intensity factor (K) crack growth rate test on a compact tension specimen of type 316 stainless steel was conducted in pure water under both subcritical and supercritical conditions.

3.1 Experiment

A 0.5 in. thick, compact tension (0.5T CT) specimen with 5% side grooves on each side was used for the crack growth rate test. This specimen was fabricated from unsensitized, type 316 stainless steel that was “cold” worked at 140°C to 21% reduction in area. At 140°C, very little or no martensite was formed during working.

Crack length was measured using the reversed direct current potential drop (DCPD) technique, which has been shown to provide accurate and reliable measurement in subcritical water [14-16]. Platinum current and potential probe leads were spot welded to the CT specimen to measure the crack length. The placement of the probe leads was optimized to obtain the best accuracy and reproducibility of the DCPD measurement, Fig. 16. A DC source supplied a stable current to the CT specimen, which was reversed periodically through solid state relays to correct for thermocouple effects. The potential drop resulting from crack extension in the specimen was measured by a nanovolt meter that averaged hundreds or thousands of individual readings. Data acquisition, data averaging, current reversal, the relationship between the measured potential and crack length, and load control for constant K experiments were controlled by dedicated software run on a PC.

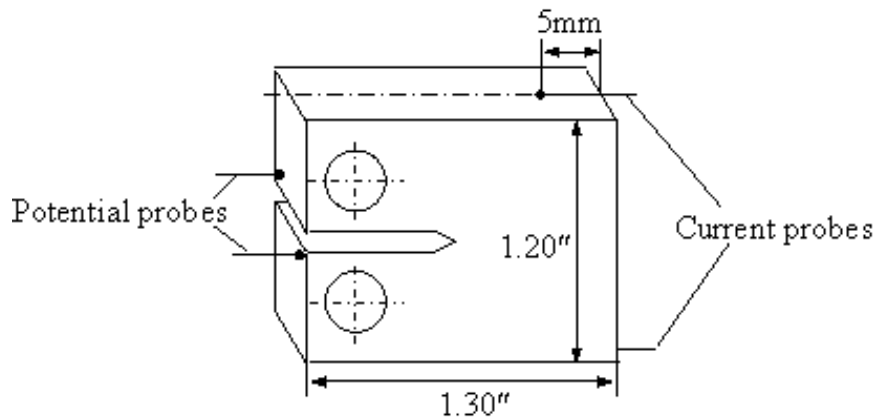


Figure 16. A schematic drawing showing the placement of the probe leads on the CT specimen.

The CT specimen was loaded by clevis pins and electrically isolated from the pins and clevises using zirconia sleeves inserted into the specimen, and zirconia washers inserted into the space between the side faces of the specimen and the clevises. The crack was initiated and

extended in air to 1.4 mm from the machined notch by a three-step fatigue program conducted at 1HZ with a load ratio (ratio of the minimum K to maximum K), R and K_{max} of 0.3 and 25.25 MPa \sqrt{m} , 0.5 and 26.35 MPa \sqrt{m} , and 0.7 and 27.45 MPa \sqrt{m} , respectively. Crack extension was continued in the environment at R = 0.7 and K_{max} = 27.45 MPa \sqrt{m} with a frequency that decreased from 0.1HZ to 0.01HZ to 0.001HZ, then by introducing a hold time of 9000s at K_{max} . These loading steps were employed to transform the cracking mode from transgranular to intergranular before switching to fully constant K at 27.45 MPa \sqrt{m} for the evaluation of the crack growth rate. The fully constant K test was performed in 288°C and 360°C subcritical water followed by 400°C, 450°C and 500°C supercritical water. During the test, sawtooth and trapezoidal waveform loading with 0.001Hz, R=0.7, K_{max} = 27.45 MPa \sqrt{m} and a hold time of 9000s (for trapezoidal waveform) were occasionally applied to the specimen to reactivate crack growth. The dissolved oxygen (DO) content of the inlet water was 2 ppm for the test in subcritical water, and continued for the 400°C test in supercritical water. Then the DO was decreased to <10 ppb to investigate the effect of DO on crack growth rate at 400°C supercritical water. The following tests at 450°C and 500°C were both performed in deaerated water.

The crack growth studies were performed in a refreshed, nickel-base alloy (625) autoclave. Water chemistry was controlled by processing distilled water through a water purification system to ensure ultra-high purity ($\sim 0.055\mu\text{S/cm}$) and routing the water into a primary glass column. Dissolved oxygen in the inlet water was controlled by bubbling either pure argon gas or a mixture of argon and oxygen in the glass column until equilibration occurred. A low pressure pump drew water from the glass column to supply the high pressure pump, and recirculated excess water back into the column for measurements of DO and conductivity of inlet water. The water exiting the autoclave was cooled down and depressurized, purified by an ion-exchanger, then measured for DO and conductivity before flowing back into the glass column. With 2 ppm of oxygen at inlet, the conductivity of water at the autoclave outlet was 0.16-0.2 $\mu\text{S/cm}$ at 288°C, 0.2-0.4 $\mu\text{S/cm}$ at 360°C and 0.3-0.5 $\mu\text{S/cm}$ at 400°C. In the deaerated condition, the conductivity of effluent water was 0.1-0.3 $\mu\text{S/cm}$ in the temperature range of 400°C to 500°C.

To reach the target temperature in the autoclave, the water was first heated by preheaters before it flowed into the autoclave. It was then maintained at the target temperature inside the autoclave by a set of thermally insulated heating bands clamped to the autoclave body. Changing temperature during the experiment generally required 1 to 2 hours. Since DCPD is very sensitive to changes in material resistivity vs. temperature, the potential obtained at the new temperature was set so that the corresponding crack length was the same as it was at the end of the previous step. To minimize the uncertainty in crack length, the crack increment during temperature increase and stabilization was estimated according to the previous crack growth rate and added to the crack length at the new temperature.

The crack growth rate was evaluated by performing a linear fit of the data obtained by the DCPD measurement. The correlation coefficients from linear regression analyses of the crack length vs. time data from which growth rates are calculated were typically >0.98.

Table 8. Summary of the crack growth rates (CGR) and conditions for the trapezoidal waveform loading and constant-K steps of the test

# of steps	Temperature	Pressure	DO	Loading	Duration	Crack increment	CGR
Step 1-1	288°C	10.3 MPa	2 ppm	Trapezoidal	189.5 hrs	0.105 mm	Started at 6.0×10^{-8} mm/s, stabilized at 2.5×10^{-7} mm/s
Step 1-2	288°C	10.3 MPa	2 ppm	Constant K	470.4 hrs	0.431 mm	2.6×10^{-7} mm/s
Step 2-1	360°C	19.3 MPa	2 ppm	Trapezoidal	95.5 hrs	0.22 mm	6.3×10^{-7} mm/s
Step 2-2	360°C	19.3 MPa	2 ppm	Constant K	175.4 hrs	0.281 mm	4.5×10^{-7} mm/s
Step 2-3	360°C	19.3 MPa	2 ppm	Trapezoidal	55.5 hrs	0.173 mm	Started at 1.1×10^{-6} mm/s, stabilized at 6.9×10^{-7} mm/s
Step 2-4	360°C	19.3 MPa	2 ppm	Constant K	92.5 hrs	0.156 mm	4.9×10^{-7} mm/s
Step 3-1	400°C	24.8 MPa	2 ppm	Constant K	74.0 hrs	0.024 mm	Started at 1.2×10^{-7} mm/s, stabilized at 5.5×10^{-8} mm/s
Step 3-2	400°C	24.8 MPa	2 ppm	Trapezoidal	140.8 hrs	0.275 mm	Started at 7.7×10^{-7} mm/s stabilized at 3.3×10^{-7} mm/s
Step 3-3	400°C	24.8 MPa	2 ppm	Constant K	167.4 hrs	0.024 mm	4.0×10^{-8} mm/s
Step 3-4	400°C	24.8 MPa	<10 ppb	Constant K	169.1 hrs	0.031 mm	Started at 4.0×10^{-8} mm/s stabilized at 6.1×10^{-8} mm/s
Step 4-1	450°C	24.8 MPa	<10 ppb	Trapezoidal	72.2 hrs	0.127 mm	Started at 6.7×10^{-7} mm/s stabilized at 3.1×10^{-7} mm/s
Step 4-2	450°C	24.8 MPa	<10 ppb	Constant K	52.5 hrs	< 0.002	$< 1 \times 10^{-8}$ mm/s
Step 4-3	450°C	24.8 MPa	<10 ppb	Trapezoidal	93.0 hrs	0.050 mm	1.45×10^{-7} mm/s
Step 4-4	450°C	24.8 MPa	<10 ppb	Constant K	149.3 hrs	~0.001	$\sim 2.4 \times 10^{-9}$ mm/s
Step 5-1	500°C	24.8 MPa	<10 ppb	Trapezoidal	73.8 hrs	0.053 mm	1.8×10^{-7} mm/s
Step 5-2	500°C	24.8 MPa	<10 ppb	Constant K	32.0 hrs	None	$< 1 \times 10^{-8}$ mm/s

[Qunjia: Check the CGR values at 400C – the CGR rates don't agree with the crack increments and the step duration.

Following the completion of the crack growth rate test, the specimen was broken by fatigue in air at room temperature. The fracture surface of the specimen was observed using Scanning Electron Microscopy (SEM) for the identification of cracking mode and validation of the DCPD measurement.

3.2 Results

Crack growth rates and conditions for each trapezoidal waveform loading and constant-K steps of the test at various temperatures are summarized in Table 8. While there was one constant-K step at 288°C and at 500°C, the program at other temperatures consisted of two or three constant-K steps that were employed following the reactivation of crack growth by sawtooth and trapezoidal waveform loading. Details of the crack growth behavior are described in the following sections.

3.2.1 Crack growth rate in subcritical water

The crack growth behavior for step 1 in 288°C water with 2 ppm DO is shown in Figure 17. Over the 470 hrs of the test, the crack grew stably at 2.6×10^{-7} mm/s for a constant K of 27.45 MPa \sqrt{m} . This result was to be compared with the value of 2.7×10^{-7} mm/s obtained with the same alloy in the same condition as measured by Andresen [17]. The good correlation between the results obtained in the two laboratories on the same alloy and for the same testing condition confirms the reliability of the DCPD system in the experimental setup.

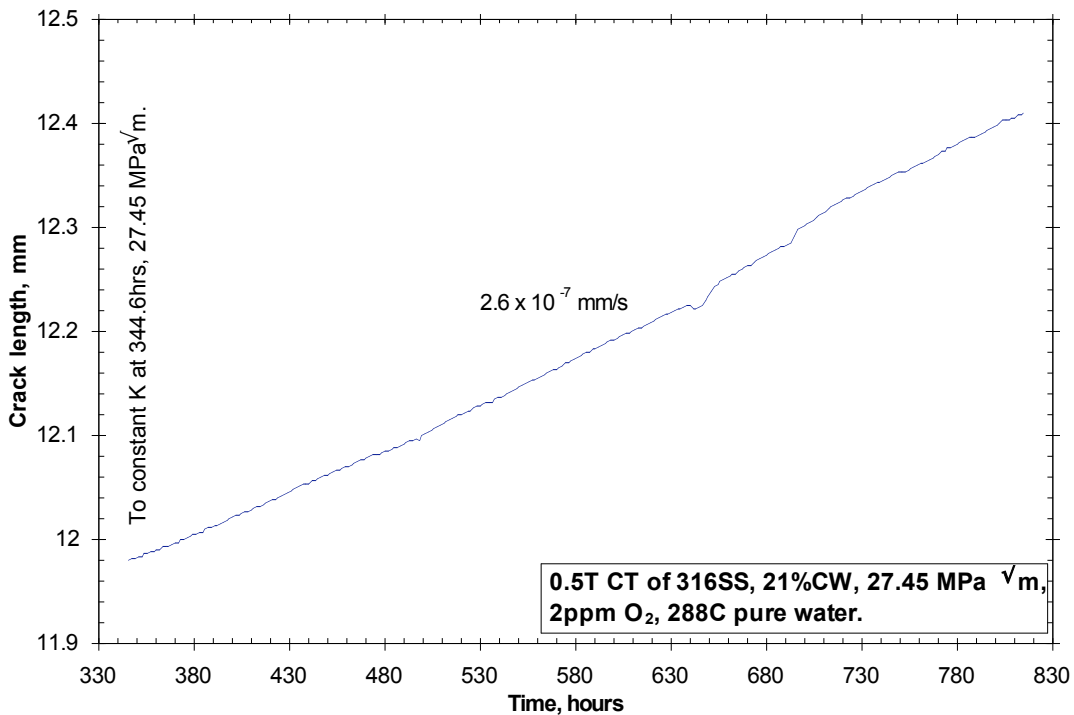


Figure 17. Crack length vs. time for a 0.5T CT specimen of unsensitized type 316L stainless steel in 288°C, oxygenated water.

Ramping the temperature of the water to 360°C caused the crack growth rate to increase. Figure 18 shows that the crack growth rate increased to 4.5×10^{-7} mm/s after switching to fully constant K at 360°C (step 2-2), which was nearly a factor of two greater than that at 288°C. The crack growth during the test must be actively managed to ensure that the SCC behavior is active and reproducible [16]. Figure 18 also gives an example on how to manage the crack growth response. Due to an unexpected unloading of the specimen, the test had to be restarted at 1871 hrs. The crack growth rate under fully constant K, however, dropped to 2.7×10^{-7} mm/s after the restart, implying that the unloading of the specimen affected the ease of crack growth. To reactivate the crack growth, trapezoidal waveform loading was applied to the specimen, causing the growth rate to increase to 7.0×10^{-7} mm/s. Returning to fully constant K at 27.45 MPa \sqrt{m} at step 2-4 then produced a stable crack growth rate of 4.9×10^{-7} mm/s that was very close to the initial growth rate of 4.5×10^{-7} mm/s.

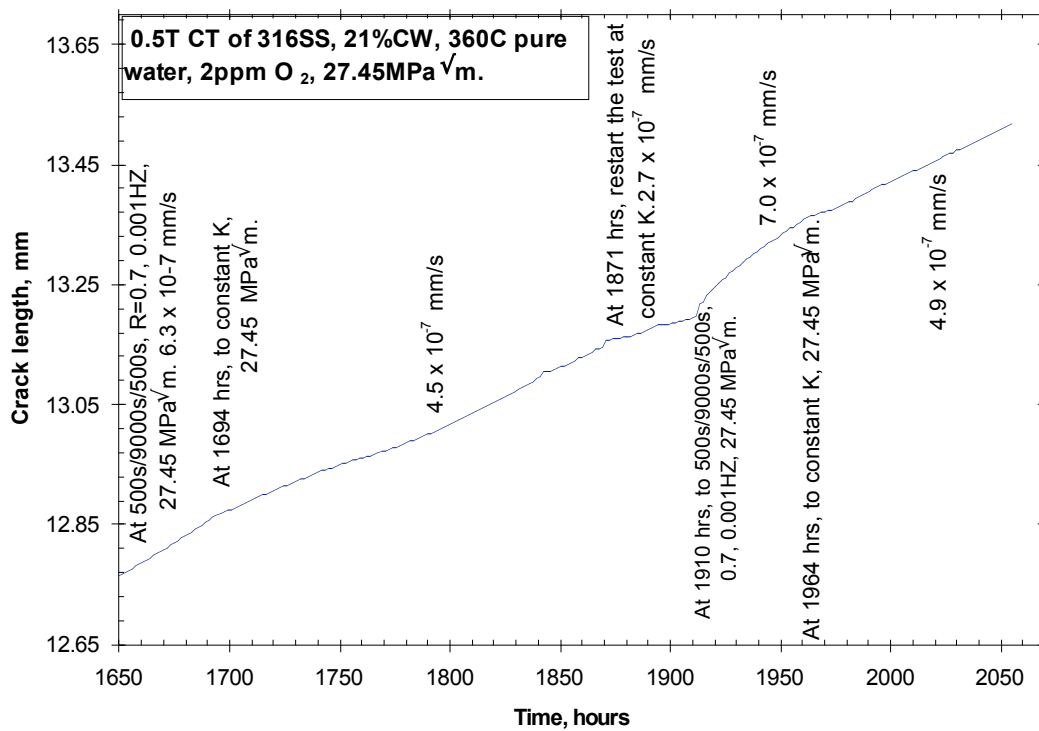


Figure 18. Crack length vs. time for a 0.5T CT specimen of unsensitized type 316L stainless steel in 360°C, oxygenated water. This figure also shows how to manage the response of crack growth to ensure an active and reproducible SCC behavior.

3.2.2 Crack growth rate in supercritical water

Increasing the temperature to 400°C at step 3-1 resulted in an immediate decrease in the crack growth rate to 1.1×10^{-7} mm/s, Fig. 19. The growth rate then further decreased to 5.5×10^{-8} mm/s. The trapezoidal waveform loading was therefore applied to the specimen in an effort to determine the activity and reproducibility of this crack growth behavior (step 3-2). The crack began to grow faster immediately and finally grew at a stable rate of 3.3×10^{-7} mm/s. Changing the loading condition back to fully constant K at step 3-2 then caused a stable, well-behaved

crack growth rate of 4.0×10^{-8} mm/s. Despite the low value, the crack growth rate in 400°C supercritical water was reproducible.

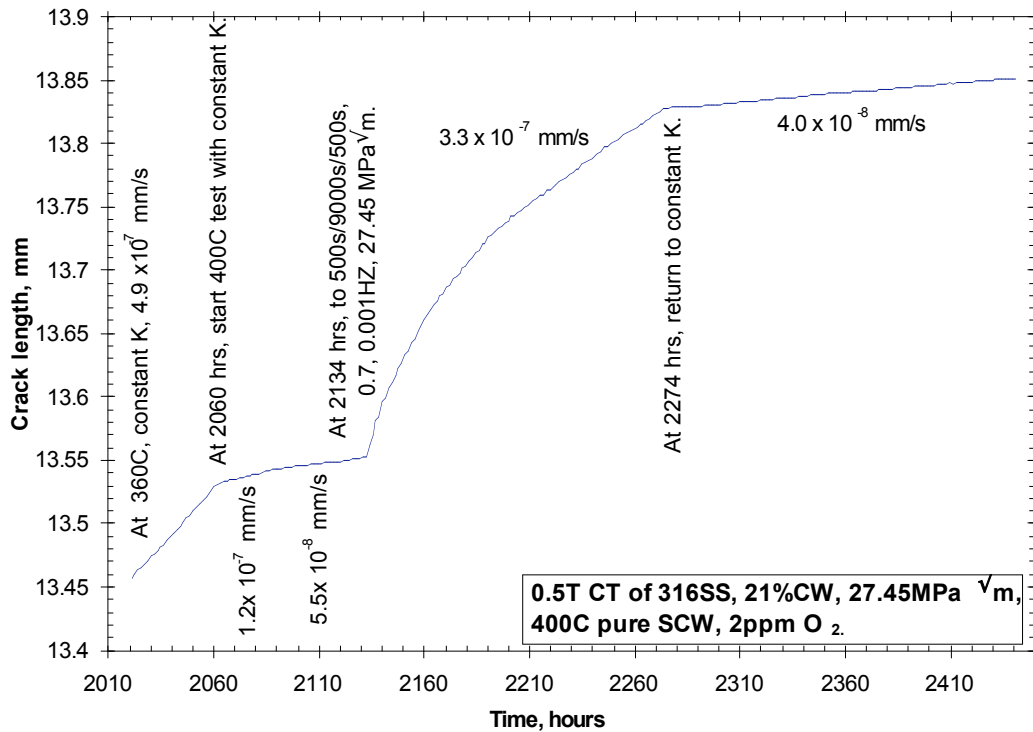


Figure 19. Crack length vs. time for a 0.5T CT specimen of unsensitized type 316L stainless steel in 400°C supercritical water with 2 ppm DO.

The dissolved oxygen concentration was reduced to <10 ppb to determine its effect on crack growth rate in 400°C supercritical water (step 3-4). As shown in Fig. 20, while the crack growth rate was stable at 4.0×10^{-8} mm/s shortly after the change in dissolved oxygen, it then increased gradually to 6.1×10^{-8} mm/s, suggesting that removing dissolved oxygen in water enhanced the crack growth.

Following the 400°C test, the water was heated up to 450°C. An initial loading mode of trapezoidal waveform at step 4-1 was applied to ensure the activity of crack growth before switching to constant K. As shown in Fig. 21, the growth rate of 3.1×10^{-7} mm/s under trapezoidal waveform loading dropped immediately after the constant K condition was reached. Over the following period of 52.5 hrs before stopping the test due to a malfunction of the preheaters, the crack growth rate was below 1×10^{-8} mm/s.

The test at 450°C was restarted with a sawtooth waveform loading of 0.001HZ and R=0.7 at 2893 hrs, Figure 22. Again, this loading mode and the following trapezoidal waveform mode were employed to obtain a better crack growth behavior before starting the constant K test. As shown in Figure 22, crack growth at a very low rate of about 2.4×10^{-9} mm/s was obtained again at constant K (step 4-4). This result as well as the result obtained before restarting the test

indicated that the crack growth rate in supercritical water at 450°C was at least one order of magnitude lower than that at 400°C.

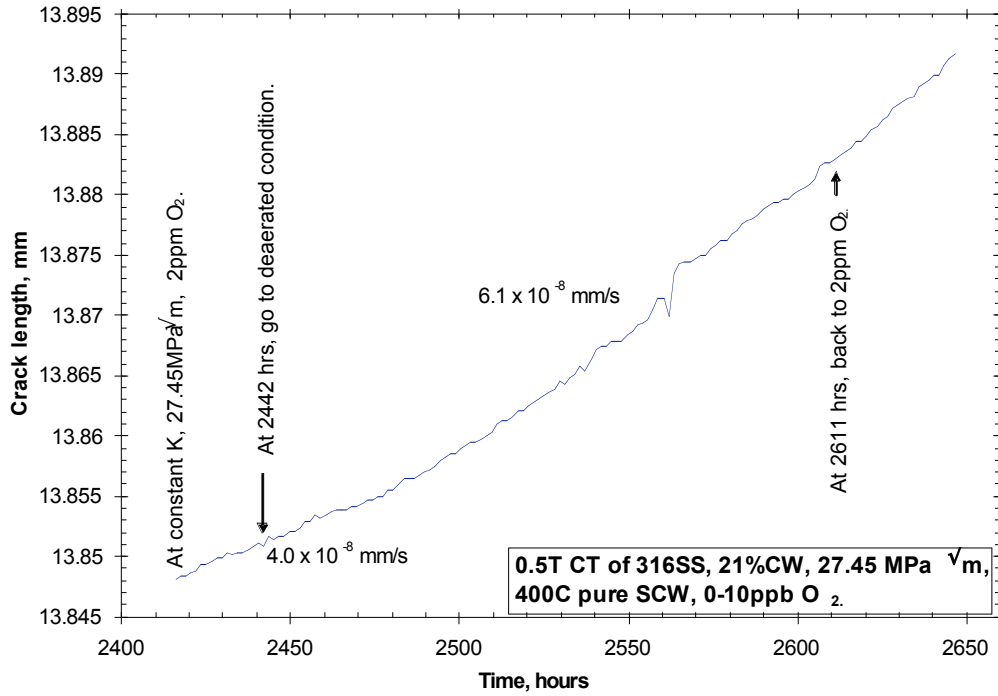


Figure 20. Crack length vs. time showing the effect of DO on crack growth rate for a 0.5T CT specimen of unsensitized type 316L stainless steel in 400°C supercritical water.

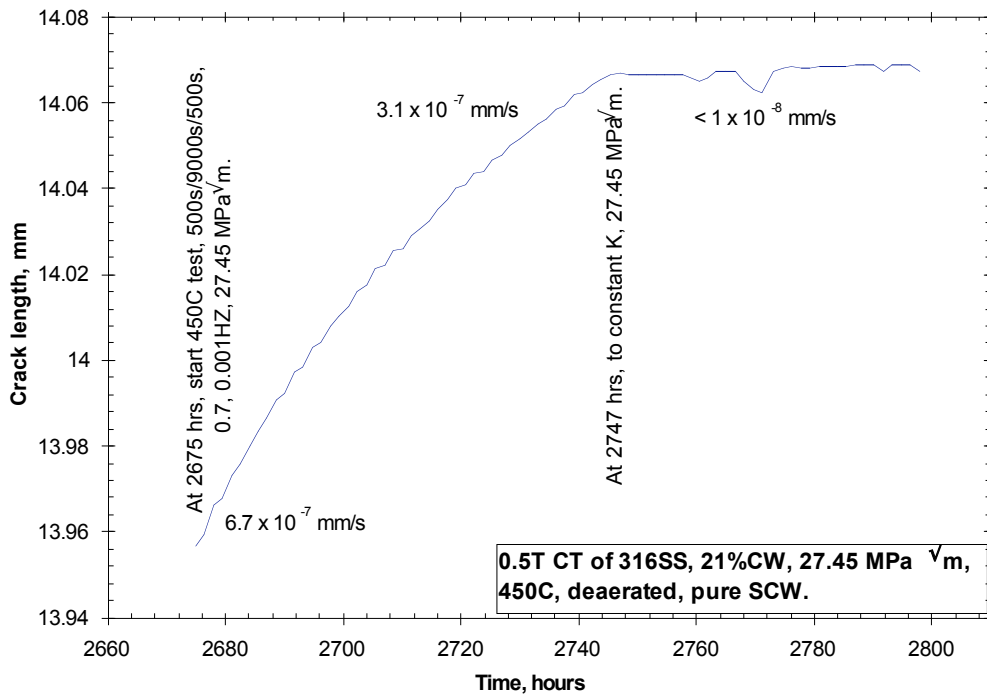


Figure 21. Crack length vs. time for a 0.5T CT specimen of unsensitized type 316L stainless steel in 450°C, deaerated supercritical water before restarting the test.

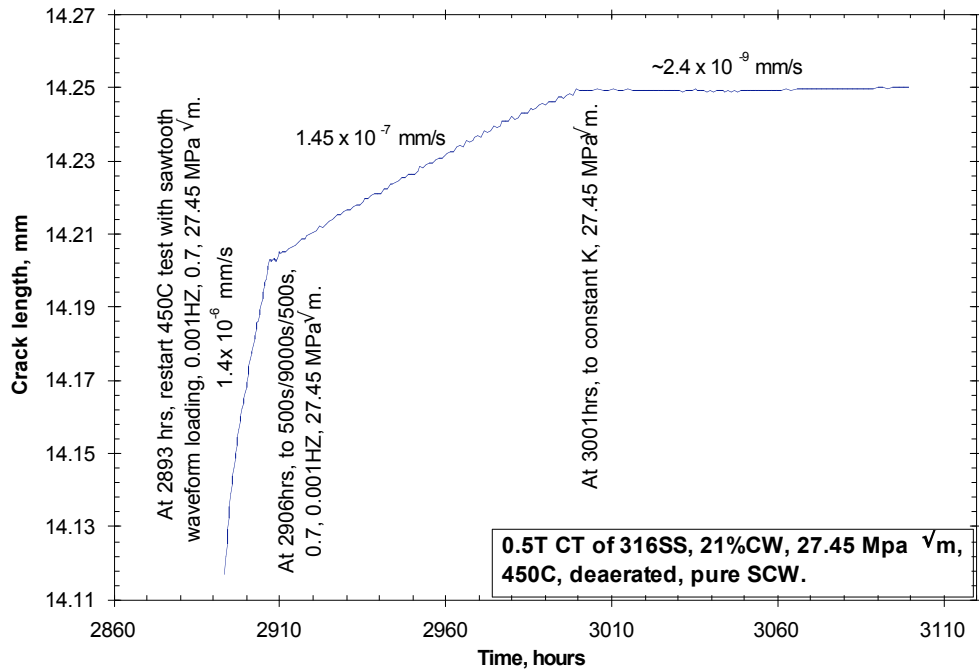


Figure 22. Crack length vs. time for a 0.5T CT specimen of unsensitized type 316L stainless steel in 450°C, deaerated supercritical water after restarting the test.

The test was then increased to 500°C, Fig. 23 and run for only 32 hr due to time limitation. No crack growth was detected for the 32 hr duration of the test, which given the resolution of the system, indicates that the growth rate must be below 1×10^{-8} mm/s.

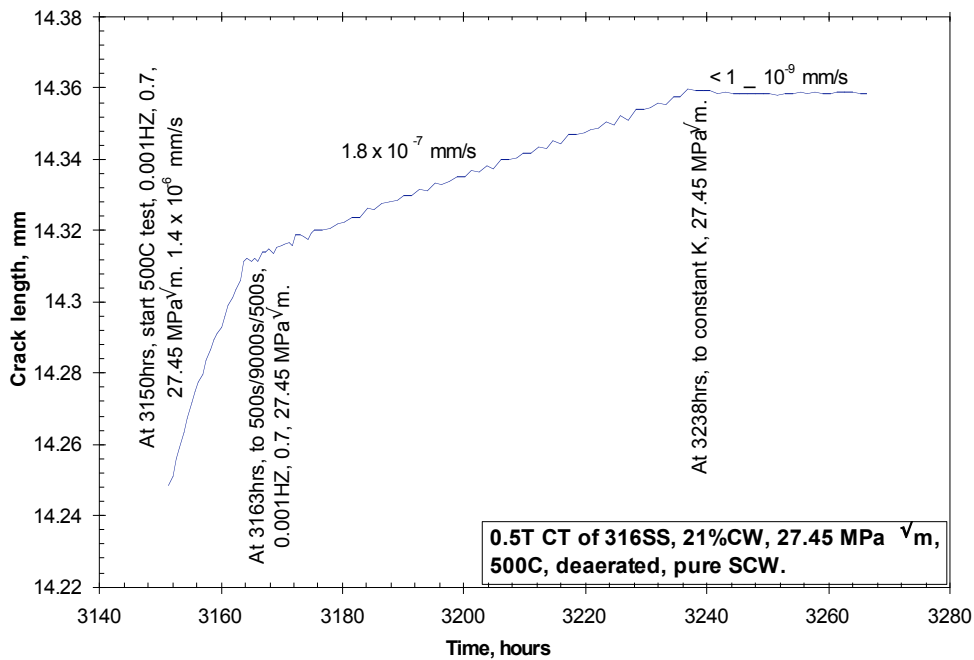


Figure 23. Crack length vs. time for a 0.5T CT specimen of unsensitized type 316L stainless steel in 500°C, deaerated supercritical water.

3.2.3 Fractography

Analysis of the crack surface using SEM revealed that it could be classified into four zones of crack propagation, Figure 24. Zones one and two exhibited typical transgranular cracking associated with fatigue pre-cracking in air. Zone three showed mixed transgranular and intergranular cracking, while zone four was typical intergranular cracking. In Fig. 25, the surface morphology for each zone is shown at high magnification.

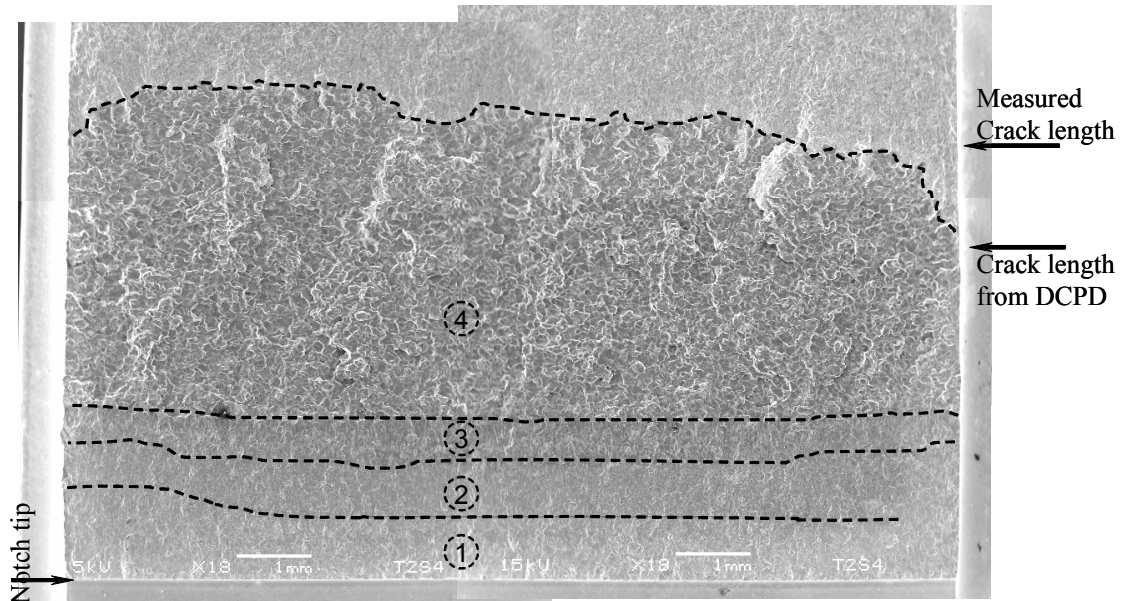


Figure 24. Fracture surface of the 0.5T CT specimen following the test. Crack extension produced during the test can be classified into four zones according to the surface morphology. Crack propagation direction is from bottom to top.

The different surface morphologies of the four zones likely resulted from the different loading modes employed during the test. The morphology of the zones suggested that they corresponded in sequence to fatigue pre-cracking in air at $R=0.3$ (zone 1), and at $R=0.5$ (zone 2), fatigue precracking in air and water at $R=0.7$ (zone 3), and intergranular crack growth produced by trapezoidal waveform and constant K loading (zone 4). The fully intergranular cracking morphology in zone 4 indicates that the SCC produced in supercritical water was completely intergranular.

The start crack length, the averaged cumulative crack length and the a/w at the end of each zone were measured on the fracture surface and are summarized in Table 9. To estimate the accuracy of the DCPD measurement of the crack length, the DCPD measurement is also listed in the table for a comparison with the fractographic crack length. The comparison in Table 9 showed that the difference between the two measurements was small (less than 30% for any zone), indicating that the DCPD measurement was valid. The errors in DCPD measurement could have been resulted from the unevenness of the crack front. Since the DCPD measurement is strongly affected by the minimum crack length on the fracture surface [14,18], the average crack length for an irregular crack front is underestimated by potential drop.

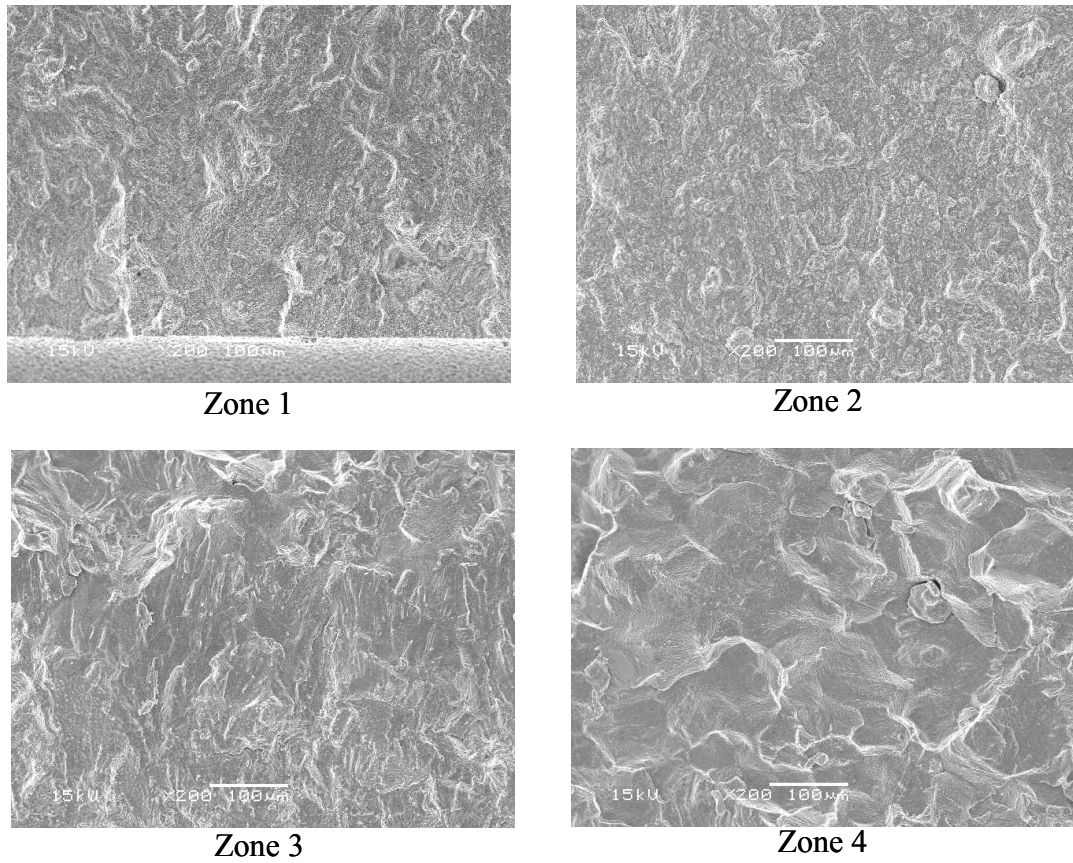


Figure 25. Crack surface morphology at higher magnification for zones 1 to 4 shown in Fig. 9.

Table 9. The start and cumulative a/w and crack lengths measured on the fracture surface at the end of each zone and comparison to that determined from DCPD measurement

# of zones	a/w	Cumulative crack length from SEM (average) (mm)	Crack length from DCPD measurement (mm)	Errors in DCPD measurement
Start (notch tip)	0.40	10.16	10.16	0
Zone 1	0.435	10.16+0.90	10.16+0.78	-13.3%
Zone 2	0.465	10.16+1.65	10.16+1.19	-27.8%
Zone 3	0.485	10.16+2.16	10.16+1.71	-20.8%
Zone 4 (final)	0.635	10.16+5.98	10.16+4.24	-29.1%

3.2.4 Validity of stress intensity factor for crack growth rate test

Several SCC relevant ASTM standards address the requirements for the specimen size to maintain linear elastic fracture mechanics conditions to eliminate the effects of specimen and crack dimensions on the measured properties such as the crack growth rate [19-21]. The validity of K at 500°C at the last step of this test was estimated. Since the yield strength of the steel is expected to be the lowest at 500°C, the K validity at this last step will ensure its validity for the whole test.

While the yield strength of our cold worked alloy at 500°C is not precisely known, 20% cold worked 316LN stainless steel has a yield strength of about 550 MPa at 450°C [22], suggesting that a yield strength of 500 MPa would be appropriate for the 21% cold worked 316 stainless steel at 500°C. Using this yield strength in conjunction with the effective thickness of the specimen (12.05 mm) and the final average crack length on the fracture surface (16.14 mm), the calculation according to E-399, a more conservative standard than others, indicated that the maximum allowable K for this test is 35 MPa $\sqrt{\text{m}}$. This value of K is almost equal to the maximum applied K at the last step of the test that calculated using the average crack length on the fracture surface, and thus the validity of K for the whole test was confirmed.

3.3 Discussion

The dependence of crack growth rate on temperature across the subcritical-supercritical line is summarized in Table 1. Typical crack growth rates at each temperature are also shown in Figure 26. In the subcritical regime, an increase in temperature from 288°C to 360°C results in an increase in the crack growth rate by a factor of about 2. The CGR increase is consistent with an activation energy for crack growth of 26 kJ/mol, which is within the range of experimentally determined values for stainless steels in high temperature water from 25°C to 288°C [18,23]. While little data exist on the crack growth rate of cold worked 316 stainless steel in 360°C water containing 2 ppm oxygen, the crack growth rate at 288°C has been well studied [14, 15, 17, 24, 25]. Experiments on the same alloy in the same condition conducted by Andresen [17] produced a crack growth rate (2.7×10^{-7} mm/s) that was nearly identical to this study (2.6×10^{-7} mm/s). As such, the crack growth behavior in subcritical water follows that expected from the existing database.

Shifting from the subcritical to the supercritical condition caused a significant drop of the crack growth rate. The crack growth rate was further suppressed by temperature increases from 400°C to 450°C and then to 500°C in supercritical water, in contrast to the increase in CGR between 288°C and 360°C. Corrosion and stress corrosion cracking in supercritical water has been observed to vary with density with greater corrosion rates at higher densities [26-30]. As shown in Fig. 26, the water density drops across the subcritical-supercritical line from 0.56 g/cm³ at 360°C to 0.17 g/cm³ at 400°C [31]. Increasing temperature to 450°C and 500°C further decreases the water density to 0.11 g/cm³ and 0.09 g/cm³ [31]. At a given temperature, the decrease in water density could reduce the corrosion rate and thus the stress corrosion crack growth rate. However, data on 316 stainless steel in SCW between 400 and 500°C exhibits an exponential increase in oxidation rate with temperature [32]. In this case, the suppression of stress corrosion crack growth rate could be related to the lower ionic solubility of the low density

supercritical water, which can cause difficulties in removing the solvated metal ions from the crack, as is necessary for the occurrence of SCC. However, this is rarely the case and it is unlikely that removal of metal ions is controlling crack growth.

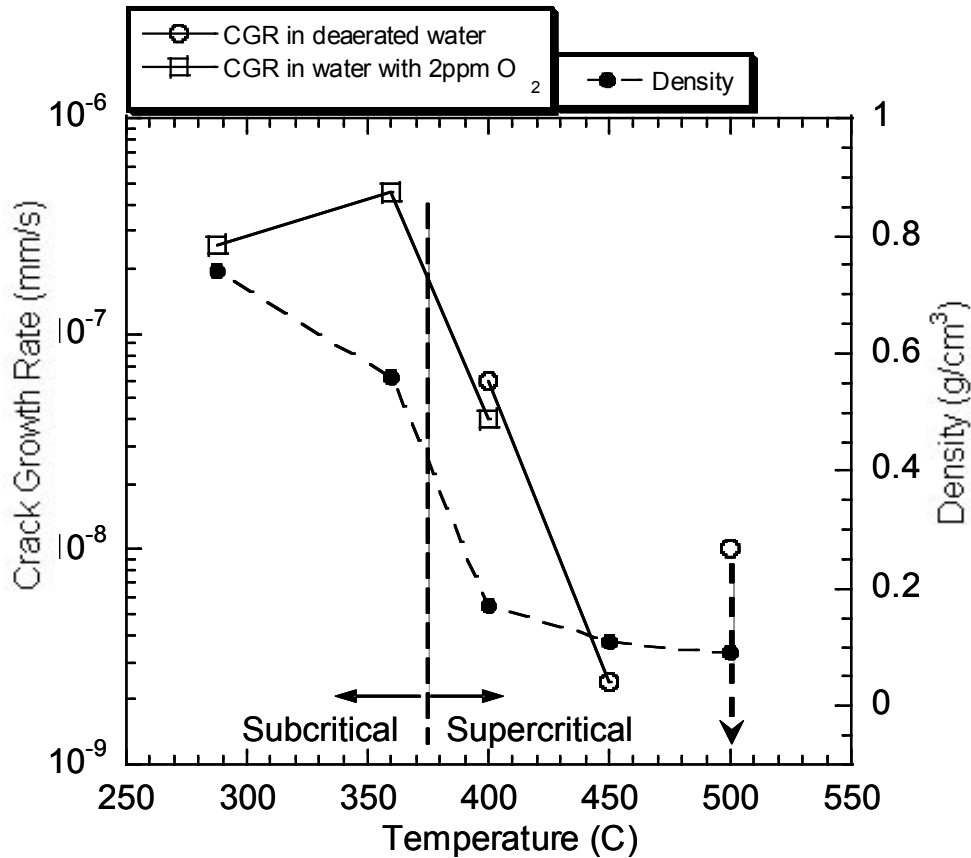


Figure 26. Crack growth rate vs. temperature across the subcritical-supercritical line for a 0.5T CT specimen of unsensitized type 316L stainless steel in pure water. The water densities at the temperature-pressure combinations of this test are also shown in the figure [31].

A more likely cause of the observed reduction of CGR in supercritical water is crack blunting due to rapid oxidation. Crack growth by slip oxidation occurs when the crack tip remains active by virtue of a higher oxidation rate at the crack tip compared to that on the crack walls, $i_{tip}/i_{walls} \gg 1$. However, at high temperature, the oxidation rate is so high that oxide growth on the crack walls will approach that at the crack tip, blunting crack growth. One test of this concept is the cracking behavior in more aggressive tests where higher strain rates prevent blunting by causing film rupture. In fact, cracking in solution annealed 316SS in deaerated SCW at 400°C and 500°C show that increasing temperature results in decreased crack density, but deeper IG cracks in constant extension rate tests, for an overall increase in IG cracking propensity in these tests [32]. While these measures of cracking are different between the two test types, collectively, they do offer an explanation for the observations. If the crack is blunted by rapid oxide growth at high temperature, then crack growth is reduced. But if the oxide is

continually ruptured due to a comparatively high strain rate, then the effect of temperature is to increase the degree of cracking.

The effect of dissolved oxygen on crack growth behavior in 400°C supercritical water shown in Fig. 20 is also likely related to the change in the oxidation rate with DO. Decreasing DO from 2 ppm to <10 ppb could reduce the rapid oxide growth rate that blunted the crack and hence resulted in higher crack growth rate.

3.4 Summary

- Stress corrosion crack growth rates in cold-worked type 316 stainless steel in pure water increased with temperature in the subcritical regime between 288°C and 360°C.
- In the supercritical regime, the crack growth rate decreased with temperature increases from 400°C to 450°C and then to 500°C. In addition, the effect of increased dissolved oxygen was to lower the crack growth rate compared to the deaerated case.
- Analysis of the fracture surface using SEM revealed that the SCC in both subcritical and supercritical water was intergranular. Comparison of the crack length from SEM and DCPD showed that the DCPD measurements of crack length are within 30% of that measured from the fracture surface.
- Crack blunting by rapid oxidation in the supercritical regime during a CGR test as opposed to film rupture by the higher strain rate of a CERT test may explain the different temperature dependence of cracking in CGR vs. CERT tests.

A summary of the project milestones is provided in Table 10.

Table 10. Project Milestone Status

Task	Subtask - Milestone	Completion Date
1. Shipping procedures	Establishment of shipping and testing procedures	12/31/05
	Shipping of samples from PNNL to UM	6/13/06
2. CERT testing of irradiated samples	CERT test in 400°C and 500°C, deaerated SCW	9/30/06
	SEM analysis of fracture surface and gage surfaces	9/30/06
3. CGR testing of unirradiated material	Establishment of CGR testing protocol	12/31/05
	CGR experiments on two unirradiated samples to provide a basis for CGR data from irradiated samples.	7/30/06

4. References

1. Code of federal Regulation, Title 49, § 173.412, US Department of Transportation, Washington DC.
2. Code of federal Regulation, Title 49, § 172.202, US Department of Transportation, Washington DC.
3. Code of federal Regulation, Title 49, § 172.203, US Department of Transportation, Washington DC.
4. Code of federal Regulation, Title 49, § 178.503, US Department of Transportation, Washington DC.
5. Code of federal Regulation, Title 49, § 172.400, US Department of Transportation, Washington DC.
6. Code of federal Regulation, Title 49, § 172.403, US Department of Transportation, Washington DC.
7. Code of federal Regulation, Title 10, § 30.41(c), US Department of Transportation, Washington DC.
8. Code of federal Regulation, Title 10, § 20.1906, US Department of Transportation, Washington DC.
9. Gerhard Erdman, “Kernchemie in Einzeldarstellungen Vol 6:Neutron Activation Tables”, Weinheim, New York, Verlag Chemie, 1976.
10. Grove Engineering, “ MicroShield User’s Manual (Version 5)”, Rockville, MD 20852, 1996.
11. N. Hashimoto et al., “ Microstructure of austenitic stainless steels irradiated at 400°C in the ORR and the HFIR spectral tailoring experiment”, J. Nucl. Mater. 280 (2000) 186-195
12. Y. Kohno et al. “Specimen size effect on the tensile properties of JPCA and JFMS”, j. Nucl. Mater. 283-287 (2000) 1014-1017.
13. G. S. Was, “Stress Corrosion Cracking of Candidate Alloys for the Supercritical Water Reactor Concept,” 2005 Annual Report.
14. P. L. Andresen and C. L. Briant, “Environmentally Assisted Cracking of Types 304L/316L/316NG Stainless Steel in 288°C Water,” Corrosion, 45(1989), 448.
15. P. L. Andresen, “Environmentally Assisted Growth Rate Response of Nonsensitized AISI 316 Grade Stainless Steels in High Temperature Water,” Corrosion, 44(1988), 450.
16. P. L. Andresen, L. M. Young and P. W. Emigh et al., “Stress Corrosion Crack Growth Rate Behavior of Ni Alloys 182 and 600 in High Temperature Water,” in: Proc. CORROSION/2002, paper No. 02510, NACE International, 2002.
17. P. L. Andresen, P. W. Emigh, M. M. Morra and R. M. Horn, “Effects of Yield Strength, Corrosion Potential, Stress Intensity Factor, Silicon and Grain Boundary Character on the SCC of Stainless Steels,,” in: Proc. 11th International Symposium on Environmental Degradation of Materials in Nuclear Power Systems-Water Reactors, ANS, 2003, pp. 816-830.
18. P. L. Andresen, “Effects of Temperature on Crack Growth Rate in Sensitized Type 304 Stainless Steel and Alloy 600,” Corrosion, 49(1993), 714.
19. “Standard Test for Plane-Strain Fracture Toughness of Metallic Materials”, E399-90, 1997 Annual Book of ASTM Standards, Volume 03.01, ASTM, 1997.
20. “Standard Test Method for Constant Load Amplitude Fatigue Crack Growth Rates”, E647-95a, 1997 Annual Book of ASTM Standards, Volume 03.01, ASTM, 1997.

21. "Standard Test Method for Determining a Threshold Stress Intensity Factor for Environment-Assisted Cracking of Metallic Materials Under Constant Load", E1681-95, 1997 Annual Book of ASTM Standards, Volume 03.01, ASTM, 1997.
22. T. S. Byun, N. Hashimoto and K. Farrell, "Temperature Dependence of Strain Hardening and Plastic Instability Behaviors in Austenitic Stainless Steels," *Acta Materialia*, 52(2004), 3889.
23. T. Haruna, S. Zhang and T. Shibata, "Analysis of Initiation and Propagation of Stress Corrosion Cracks in Sensitized Type 304 Stainless Steel in High-Temperature Water," *Corrosion*, 60(2004), 1104
24. P. L. Andresen, P. W. Emigh, M. M. Morra and R. M. Horn, "Effects of Yield Strength, Corrosion Potential, Stress Intensity Factor, Silicon and Grain Boundary Character on the SCC of Stainless Steels", in: Proc. 11th International Symposium on Environmental Degradation of Materials in Nuclear Power Systems – Water Reactors, ANS, 2003.
25. P. L. Andresen, L. M. Young, W. R. Catlin and R. M. Horn, "Stress Corrosion Crack Growth Rate Behavior of Various Grades of Cold Worked Stainless Steel in High Temperature Water", in: Proc. CORROSION/2002, Paper No. 02511, NACE International, 2002.
26. P. Kritzer, "Corrosion in High-temperature and Supercritical Water and Aqueous Solutions: A Review," *The Journal of Supercritical Fluids*, 29(2004), 1.
27. L. B. Kriksunov and D. D. Macdonald, "Corrosion in Supercritical Water Oxidation Systems: a Phenomenological Analysis," *J. Electrochem. Soc.*, 142 (1995), 281.
28. K. Sue, N. Tsujinaka and T. Adschiri et al., "Relationship between Corrosion Rate and Metal Oxide Solubility in Supercritical Water," in: Proc. CORROSION/2002, Paper No. 02354, NACE International, 2002.
29. Y. Watanabe, T. Kobayashi and T. Adschiri, "Significance of Water Density on Corrosion Behavior of Alloys in Supercritical Water," in: Proc. CORROSION/2001, Paper No. 01369, NACE International, 2001.
30. H. Abe, Y. Watanabe and K. Sue, "Stress Corrosion Cracking Mechanisms of 316 Stainless Steels in Sub-Critical Liquid Water and Supercritical Water from a "Dielectric Constant of Water" Point of View", in: Proc. ICAPP'04, paper 4226, June 2004, Pittsburgh, PA USA.
31. W. Wagner and A. Prub, "The IAPWS Formulation 1995 for the Thermodynamic Properties of Ordinary Water Substance for General and Scientific Use," *J. Phys. Chem. Ref. Data*, 31(2002), 387.
32. G. S. Was and S. Teysseyre, *Corrosion*, in press.